8 Some Mathematical & Conceptual Tools: Part 2. Time Series

Spectrum analysis is a statistical tool that we can employ to probe further into the workings of turbulence. By decomposing a series of measurements into frequency or wavenumber components, we can discover how eddies of different time and space scales contribute to the overall turbulence state.

In this chapter we review the computational techniques for the spectrum analysis of measured data. We also introduce related tools such as the autocorrelation function, structure function, and periodogram. Also discussed is the concept of a process spectrum, where mixing processes rather than turbulence states are decomposed into a spectrum of scales. Theoretical spectral decomposition of the TKE equation is briefly covered.

8.1 Time and Space Series

When measurements are taken at a fixed point over a period of time, the resulting series of data points is called a ***time series***. Similarly, measurements at a fixed time over a series of locations in space is called a ***space series***. Both series give measurements of a dependent variable such as temperature or humidity as a function of an independent variable, such as time, t, or location, x. Because of this similarity, we will discuss the two types of series interchangeably, and sometimes will use the generic name, ***series***.

This review will be limited to ***discrete*** series; namely, measurements taken at regularly-spaced intervals that lead to a finite number, N, of data points. A discrete series represents a ***sample*** of the true, continuously-varying signal. Examples of discrete series include temperature or tracer concentration measurements made every second during the course of an hour at a fixed location such as an instrumented tower, or measurements of humidity taken every meter from an aircraft flying on a 25 km flight leg.

If A(t) represents the true signal as a continuous function of time, then we could sample that signal at evenly-spaced times: $t = t_o$, $t = t_o+\Delta t$, $t = t_o+2\Delta t$, $t = t_o+3\Delta t$, ..., $t = t_o+(N-1)\Delta t$, where the total number of data points is N. We will use an ***index***, k, to denote the position within the time series. The k^{th} data point corresponds to time $t_k = t_o + k\Delta t$, where $0 \le k \le (N-1)$. Sometimes the value of variable A at time t_k is represented by $A(t_k)$, but usually the shorthand notations A(k) or A_k is used. We will assume that the ***sampling interval*** is Δt, with no missing data and no changes of Δt within any one series. The ***total period*** of measurements is $\mathbb{P} = N\Delta t$, in the sense that each of the N data points represents a sample within an interval Δt.

8.2 Autocorrelation

In section 2.4.5 we discussed the covariance and the correlation coefficient, which quantify the amount of common variation between two different variables. Extending this idea, we could also ask about the degree of common variation between a variable (A) sampled at time t and that same variable sampled at a later time, t+L, where L is the time lag. Such a correlation of a variable with itself is called ***autocorrelation***, $R_{AA}(L)$.

Consider a 12 hour time series that has a simple sinusoidal variation of unit amplitude with a 4 hour period. The wave equals 1.0 at regular intervals of 1, 5, and 9 h. Also, the wave equals -1.0 at 3, 7, and 11 h. In fact at ANY time, t, the series is perfectly correlated with itself (i.e., has the same value) at exactly times t + 4 h, t + 8 h, and t + 12 h. Similarly, we can show that the wave is negatively correlated with itself at t + 2 h, t + 6 h, and t + 10 h. We have, in essence, just determined the autocorrelation for this series at lags 2, 4, 6, 8, 10, and 12 h.

If our time series consists of a wave that varies in frequency during the duration of the series, then a wave at t_1 might be perfectly correlated with itself at $t_1 + 4$ h, but the value at t_2 might not be perfectly correlated with the value at $t_2 + 4$ h. When averaged over all possible pairs of data points with 4 h lag in this series, the result might NOT give a large correlation value at all.

In other words, the autocorrelation measures the persistence of a wave within the whole duration a time or space series. The capability to determine persistent waves or oscillations within a series is particularly valuable because the regular variation might be associated with a physical phenomenon such as an eddy. Alternately, when the autocorrelation becomes close to zero, it tells us that there is a random process (e.g. turbulence) occurring with no persistent or regularly-recurring structures.

8.2.1 Definition

The exact definition for the discrete autocorrelation is:

$$R_{AA}(L) = \frac{\sum_{k=0}^{N-j-1}\left[(A_k - \overline{A}_k)(A_{k+j} - \overline{A}_{k+j})\right]}{\left[\sum_{k=0}^{N-j-1}(A_k - \overline{A}_k)^2\right]^{1/2}\left[\sum_{k=0}^{N-j-1}(A_{k+j} - \overline{A}_{k+j})^2\right]^{1/2}} \qquad (8.2.1a)$$

where two different mean values are used depending on which portion of the whole series is being considered:

$$\overline{A}_k = \frac{1}{N-j}\sum_{k=0}^{N-j-1} A_k \qquad \text{and} \qquad \overline{A}_{k+j} = \frac{1}{N-j}\sum_{k=0}^{N-j-1} A_{k+j}$$

and where lag = L = j Δt. Notice that each of the square bracket terms in the denominator acts like a standard deviation over the portion of the data set being used.

We can approximate (8.2.1a) if it is assumed that the data is sufficiently stationary (or homogeneous for space series) that the mean values over each portion of the series is equal to the overall series mean, and that the standard deviations from each portion equal the overall series standard deviation. This results in:

$$R_{AA_{approx}}(L) = \frac{\overline{A_k' A_{k+j}'}}{\sigma_A^2} \qquad (8.2.1b)$$

This simple approximation works satisfactorily for small lags (i.e., small j) and large N, but is inadequate otherwise.

Autocorrelations are usually calculated for a range of lags, and the result plotted on a graph of R_{AA} vs L. For the special case of zero lag, the autocorrelation is identically equal to unity [$R_{AA}(0) = 1.0$] for all signals. The autocorrelation of an irregular signal such as turbulence approaches zero as L approaches infinity, although it may appear as damped oscillations about zero while L is small. Also, as the lag increases, the percentage of the time series used to calculate $R_{AA}(L)$ decreases. As a result, the statistical significance of R_{AA} decreases as lag increases, making R_{AA} unrepresentative when $j > (N/2)$.

Sample autocorrelation curves for convective turbulence measured at different heights in the ML are shown in Fig 8.1 (Deardorff and Willis, 1985).

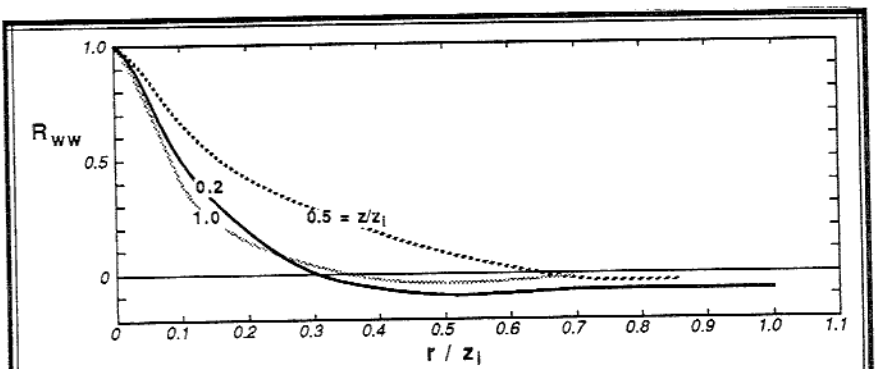

Fig. 8.1 Autocorrelation of vertical velocity in a ML as a function of separation distance **r** (spatial lag) and height z, based on the laboratory simulation of Deardorff and Willis (1985).

8.2.2 Example

Problem: Given the following series of measurements of relative humidity made every 3 h over a 96 h period (4 days) at a fixed point. Find the autocorrelation for relative humidity, $R_{rh,rh}(L)$, for time lags ranging from 0 to 48 hours, and plot the result.

Data:

	Relative humidity (percent)							
Day 1:	49	46	44	45	52	59	61	57
Day 2:	53	50	50	52	55	55	54	47
Day 3:	41	36	32	33	36	41	40	37
Day 4:	34	31	29	32	38	45	48	45

As can be seen in a plot of the time series (Fig 8.2a), there are regular diurnal cycle oscillations superimposed on longer period trends.

Solution: There are 32 data points, with Δt = 3 h. We must solve (8.2.1) 17 different times, for j = 0 through j = 16. The result is:

L(h)	$R_{rh,rh}$	L(h)	$R_{rh,rh}$	L(h)	$R_{rh,rh}$	L(h)	$R_{rh,rh}$	L(h)	$R_{rh,rh}$	L(h)	$R_{rh,rh}$
0	1.00	9	0.35	18	0.49	27	0.34	36	-0.13	45	0.40
3	0.67	12	0.34	21	0.53	30	0.09	39	-0.04	48	0.58
6	0.47	15	0.40	24	0.50	33	-0.12	42	0.17		

Discussion: Looking at Fig 8.2b, we see that the autocorrelation starts at 1.0 at zero lag, and quickly decreases. As is sometimes the case with weather data, the diurnal cycle shows up as an oscillation in the autocorrelation function with a 24 hour period. We could have anticipated this, because 12 h from any time, the humidity time series is in the

opposite side of its oscillation. If the humidity is high in the early morning, then 12 h later it is drier. If the humidity is low in the afternoon, then 12 h later it is more humid. On the average, humidity is negatively correlated with itself 12 h later. Over a 24 h period, however, like comparing a morning humidity with the next morning's humidity, or the afternoon humidity with the next afternoon's humidity, we anticipate a positive correlation.

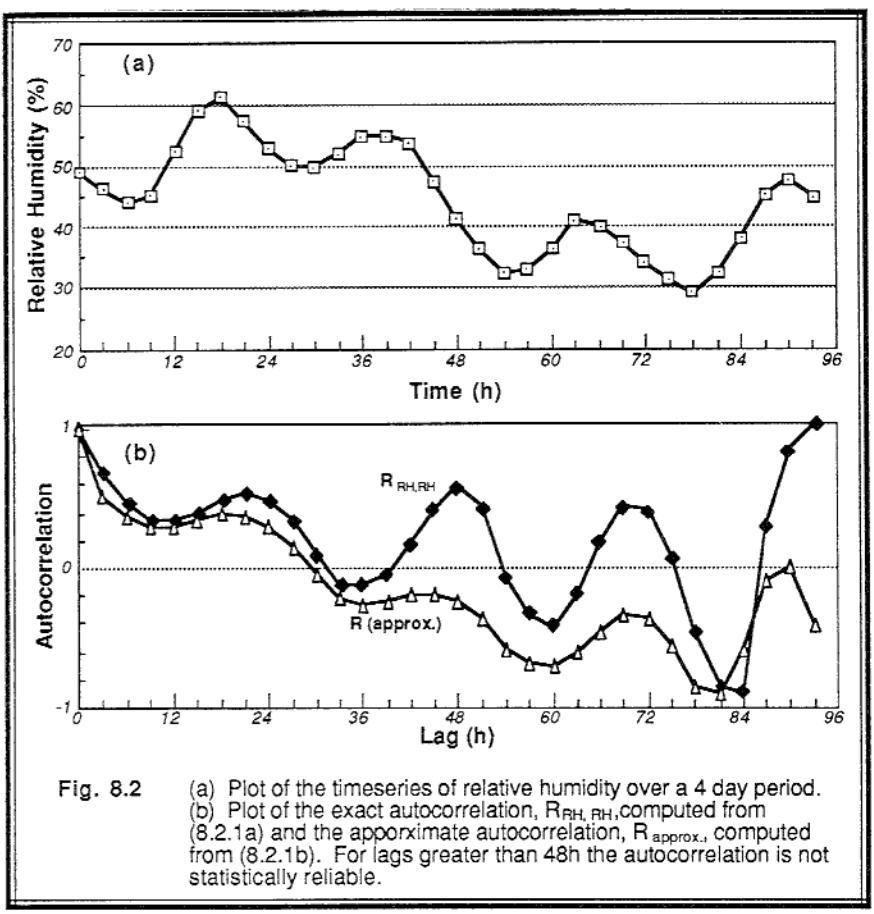

Fig. 8.2 (a) Plot of the timeseries of relative humidity over a 4 day period. (b) Plot of the exact autocorrelation, $R_{RH,RH}$, computed from (8.2.1a) and the apporximate autocorrelation, $R_{approx.}$, computed from (8.2.1b). For lags greater than 48h the autocorrelation is not statistically reliable.

The initial drop off of the autocorrelation from 1.0 to smaller values is a measure of the accuracy of a persistence forecast. Namely, if we forecast the humidity 3 or less hours from now to be the same as the present humidity, we would probably be close to correct because the autocorrelation is 60% or higher. Longer forecasts would be less accurate.

8.3 Structure Function

8.3.1 Definition

An alternative statistic to view common variation is the ***structure function***, $D_{AA}(L)$:

$$D_{AA}(L) = \frac{1}{N}\sum_{k=0}^{N-1}\left[A_k - A_{k+j}\right]^2 \qquad (8.3.1a)$$

For a time series, $L = j\,\Delta t$ is the time lag, while for a space series $L = \mathbf{r} = j\,\Delta r$ represents the spatial separation, **r**, between the two measurements. The structure function uses the difference, rather than the product, of two different points in the series. The structure function has units of A^2 like variance, rather than being dimensionless like the autocorrelation.

For zero lag or zero separation distance, the structure function is identically zero. As L or **r** increases, so does the structure function for most turbulent flows. Within the inertial subrange of turbulence, similarity arguments (similarity theory is reviewed in Chapter 9) suggest that:

$$D_{AA}(\mathbf{r}) = c_{A^2}\,\mathbf{r}^{2/3} \qquad (8.3.1b)$$

where c_{A^2} is the ***structure function parameter*** for variable A. The four most common structure function parameters are c_{T^2} for temperature, c_{V^2} for velocity, c_{q^2} for moisture, and c_{nref^2} for the index of refraction, n_{ref}. These parameters are not dimensionless, but have units determined by the units of A and **r** to make (8.3.1b) dimensionally consistent (see example below).

Remote sensors such as radar (microwaves) or sodar (sound) can receive returns from clear air because some of the transmitted signal is scattered off of refractive index variations in the atmosphere. For example, the radar reflectivity η (radar cross section per unit volume) in clear air (no rain or other hydrometeors) is:

$$\eta = 0.38\, c_{nref^2}\, \lambda_R^{-1/3} \qquad (8.3.1c)$$

where λ_R is the wavelength of the radar. Since the index of refraction is related to temperature, moisture, and pressure to varying degrees depending on the type of remote sensor, equations can be derived relating c_{nref^2} to c_{T^2}, c_{q^2} and c_{V^2} (see review by Lenschow, 1986). Thus, the magnitude of the returned signal η gives c_{nref^2} from (8.3.1c), which yields estimates of c_{T^2}, c_{q^2} and c_{V^2}. Sample profiles of c_{T^2} and c_{V^2}

are shown in Fig 8.3.

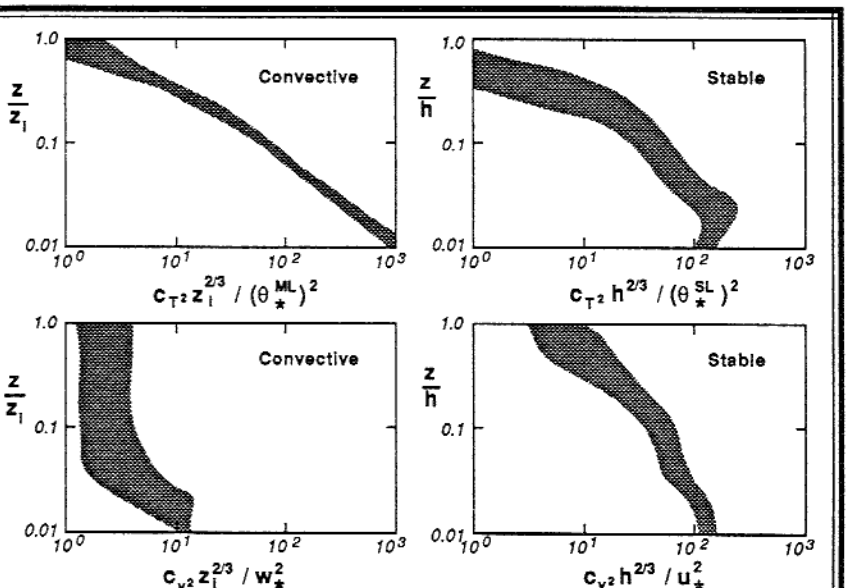

Fig. 8.3 Profiles of c_{T^2} and c_{v^2} in convective and stable conditions, normalized by mixed layer and surface-layer scaling parameters. After Neff and Coulter (1986).

Remote sensors can yield a variety of quantitative boundary layer information, utilizing the structure function statistic. We can estimate dissipation rates because similarity arguments suggest that:

$$c_{V^2} = 2\,\varepsilon^{2/3} \qquad \text{and} \qquad c_{T^2} = a^2\,\varepsilon_\theta\,\varepsilon^{-1/3} \tag{8.3.1d}$$

for the inertial subrange, where a^2 is a constant of about 3.0 (estimates in the literature range from 2.8 to 3.2). Wyngaard, et. al. (1971) demonstrate that surface turbulent heat flux in the ML can be calculated from c_{T^2} :

$$c_{T2} = 2.68 \left(\frac{g}{\overline{T}}\right)^{-2/3} \cdot \left(\frac{z}{\overline{w'\theta'}_s}\right)^{-4/3} \tag{8.3.1e}$$

Wyngaard and LeMone (1980) further suggest that the magnitude of the temperature and moisture jumps across the capping inversion at the top of the ML can also be measured from c_{T^2} and c_{q^2} .

8.3.2 Example

Problem: Given the same time series of relative humidity (rh) as in example 8.2.2, calculate the structure function for lags from 0 - 48 hours.

Solution: Using (8.3.1a), the structure function values (in units of relative humidity percentage squared) are:

L (h)	$D_{rh,rh}$	L(h)	$D_{rh,rh}$	L(h)	$D_{rh,rh}$	L(h)	$D_{rh,rh}$
0	0	15	153	27	183	39	301
3	78	18	134	30	243	42	303
6	124	21	127	33	299	45	326
9	155	24	142	36	316	48	377
12	162						

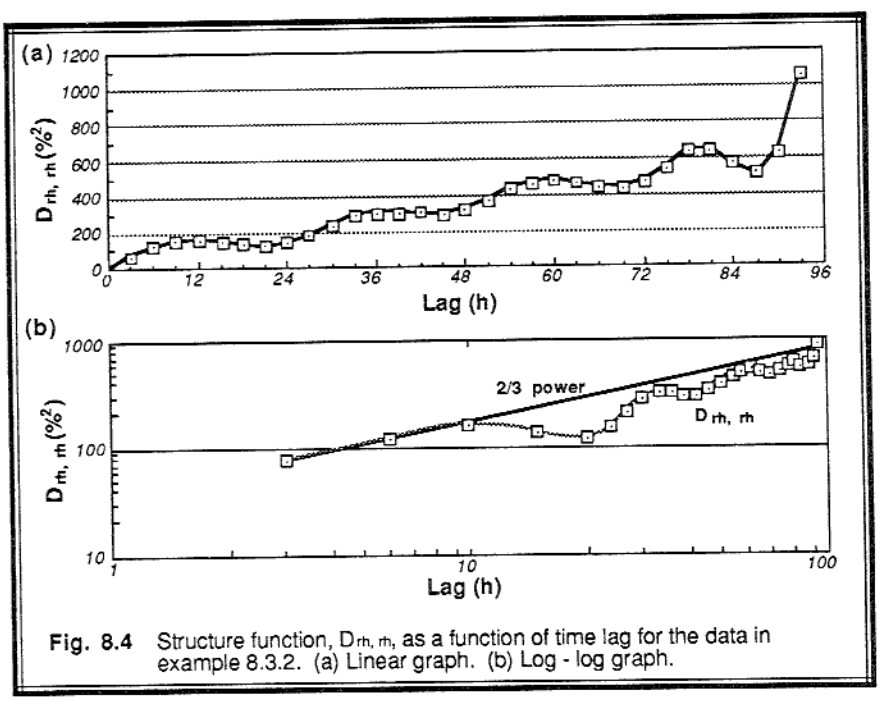

Fig. 8.4 Structure function, $D_{rh,rh}$, as a function of time lag for the data in example 8.3.2. (a) Linear graph. (b) Log - log graph.

Discussion: Fig 8.4a shows the resulting variation of the structure function on a linear scale. A similar plot on log-log graph is given in Fig 8.4b. The straight line on this latter graph is given by $D_{rh,rh} = c_{rh^2}\ L^{2/3}$, with the structure function for relative humidity $c_{rh^2} = 35\ (\%^2 \cdot h^{-2/3})$.

8.4 Discrete Fourier Transform

From Fourier analysis in calculus we remember that any well-behaved continuous function can be described by an infinite Fourier series — namely, the sum of an infinite number of sine and cosine terms. In the case of a discrete time series with a finite number of points, we are required to have only a finite number of sine and cosine terms to fit our points exactly.

8.4.1 Definition

Using Euler's notation [$\exp(ix) = \cos(x) + i \sin(x)$, where i is the square root of -1] as a shorthand notation for the sines and cosines, we can write the discrete Fourier series representation of A(k) as:

$$\text{Inverse Transform:} \qquad A(k) = \sum_{n=0}^{N-1} F_A(n)\, e^{i\,2\pi nk/N} \qquad (8.4.1a)$$

where n is the frequency, and $F_A(n)$ is the ***discrete Fourier transform.*** We see that a time series with N data points (indexed from k=0 through N-1) needs no more than N different frequencies to describe it (actually, it needs less than N, as will be shown later).

There are a number of ways to describe frequency:

n = number of cycles (per time period $\mathbb{P}$),
$\tilde{n}$ = cycles per second = $n/\mathbb{P}$,
f = radians per second = $2\pi n/\mathbb{P} = 2\pi n/(N\Delta t)$.

A frequency of zero (n = 0) denotes a mean value. The ***fundamental frequency***, where n = 1, means that exactly one wave fills the whole time period, $\mathbb{P}$. Higher frequencies correspond to ***harmonics*** of the fundamental frequency. For example, n = 5 means that exactly 5 waves fill the period $\mathbb{P}$.

$F_A(n)$ is a complex number, where the real part represents the amplitude of the cosine waves and the imaginary part is the sine wave amplitude. It is a function of frequency because the waves of different frequencies must be multiplied by different amplitudes to reconstruct the original time series. If the original time series A(k) is known, then these coefficients can be found from:

$$\text{Forward Transform:} \qquad F_A(n) = \sum_{k=0}^{N-1} \left[\frac{A(k)}{N}\right] e^{-i\,2\pi nk/N} \qquad (8.4.1b)$$

Notice the similarity between (8.4.1a) and (8.4.1b). These two equations are called ***Fourier transform pairs.*** The second equation performs the ***forward transform***, creating a representation of the signal in ***phase space*** (another name for the frequency

or spectral domain). This process is also known as ***Fourier decomposition***. The first equation performs the ***inverse transform***, converting from frequencies back into ***physical space***.

8.4.2 Example

Problem: Given the following 8 data points of specific humidity, q, as a function of time:

Index (k):	0	1	2	3	4	5	6	7
Time (UTC):	1200	1215	1230	1245	1300	1315	1330	1345
q (g/kg):	8	9	9	6	10	3	5	6

Perform a forward Fourier transform to find the 8 coefficients, $F_q(n)$. To check your results, perform an inverse transform to confirm that the original time series is recreated. Remember that the $F_q(n)$ coefficients are complex, each having a real and an imaginary part: $F_q(n) = F_{real}(n) + i\,F_{imag}(n)$.

Solution: $N = 8$ and $\Delta t = 15$ min. Thus, the total period is $\mathbb{P} = N\Delta t = 2$ h. Equation (8.4.1b) must be used to find $F_q(n)$. For those computer languages that accept complex numbers, (8.4.1b) can be programmed directly, where each of the A(k) data points has a real part equal to the value listed in the table, and an imaginary part of zero.

For hand calculation, we can use Euler's formula to translate (8.4.1b) back into sines and cosines:

$$F_A(n) = \frac{1}{N}\sum_{k=0}^{N-1} A(k)\cos(2\pi nk/N) \; - \; \frac{i}{N}\sum_{k=0}^{N-1} A(k)\sin(2\pi nk/N)$$

As an example, for n = 0, all of the cosines of zero are unity and all of the sines are zero. This leaves:

$$F_A(0) = \frac{1}{N}\sum_{k=0}^{N-1} A(k)$$

which is just the mean of A. For our case: $F_q(0) = 7.0 - 0.0\,i$. For n = 1 we can't make such a simplification, so we are forced to sum over all k for both the real and imaginary parts. This gives us $F_q(1) = 0.28 - 1.03\,i$. Continuing this procedure for all other n yields:

n	$F_q(n)$	n	$F_q(n)$
0	7.0	4	1.0
1	0.28 - 1.03 i	5	-0.78 + 0.03 i
2	0.5	6	0.5
3	-0.78 - 0.03 i	7	0.28 + 1.03 i

This is the answer to the first part of the problem. Note that for frequencies greater than 4, the Fourier transform is just the complex conjugate of the frequencies less than 4.

As a check of our transform, we can perform the inverse transform using (8.4.1a) directly in a computer program. Otherwise, we can use Euler's formula to write it as:

$$A(k) = \sum_{n=0}^{N-1} F_{(\text{real part})}(n) \cdot \cos(2\pi nk/N) - \sum_{n=0}^{N-1} F_{(\text{imag.part})}(n) \cdot \sin(2\pi nk/N)$$

In actuality, there are four sums, not just the two listed above. The remaining sums consist of the real part of F times the imaginary factor $i \cdot \sin(...)$, and the imaginary part of F times the real factor $\cos(...)$. Because the last half of the Fourier transforms are the complex conjugates of the first half (not counting the mean), these two sums identically cancel, leaving the two listed above. Upon performing the calculations for A(k), we do indeed reproduce the original time series.

Discussion: To graphically demonstrate that the sum of these sines and cosines does indeed equal our original series, Fig 8.5 shows each individual wave multiplied by its appropriate amplitude. As can be seen, the reconstructed time series fits perfectly the eight original data points. In between these points, however, the sum oscillates in a manner that is not necessarily realistic, but which is irrelevant because it occurs below the discretization resolution specified by the original data points.

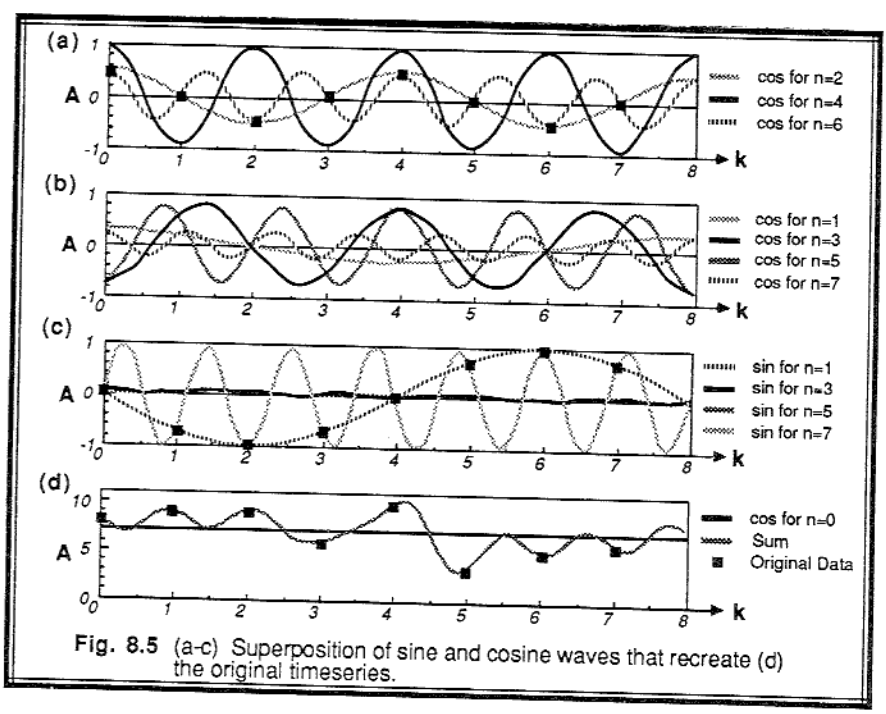

Fig. 8.5 (a-c) Superposition of sine and cosine waves that recreate (d) the original timeseries.

8.4.3 Aliasing and Other Hazards.

Measurements: A basic rule of discrete data analysis is that at least two data points are required per period or wavelength in order to resolve a wave. Since Fourier analysis involves splitting arbitrary signals into waves, the two data point requirement also holds for our arbitrary signals. For example, if we have a total of N data points, then the highest frequency that can be resolved in our Fourier transform is $n_f = N/2$, which is called the ***Nyquist frequency***. These requirements apply to measurements; namely, if a wave period as small as 0.1 s must be measured while flying in an aircraft, then the physical signal must be digitized at least once every 0.05 s. Similarly, if a wavelength as small as 1 m must be measured, then the physical signal must be digitized at least once every 0.5 m.

What happens when there is a physical signal of high frequency that is not sampled or digitized frequently enough to resolve the signal? The answer is that the true high-frequency signal is ***folded*** or ***aliased*** into a lower frequency, creating an erroneous and deceiving Fourier transform. This is illustrated with aid of the example in the previous subsection. Look at the first graph in Fig 8.5, where the cosine waves for n = 2, 4 and 6 are plotted. Since we started with N = 8 data points, we can anticipate a Nyquist frequency of $n_f = 4$. Namely, the shortest period wave that can be resolved is one that has 4 cycles per period $\mathbb{P}$. Thus, the curve corresponding to n = 6 is greater than the Nyquist frequency, and is likely to cause problems.

Look closely at the curves for n = 2 and n = 6. They coincide exactly at the points k = 0, 1, 2, 3, 4, 5, 6 and 7. In other words, if there were a true signal of n = 6 that was sampled only at the integer k values listed above, then anyone connecting the resulting plotted points with a line or curve would find that they have drawn a wave with n = 2 cycles per period. In other words, the n = 6 signal was folded into the n = 2 frequency. Similarly, looking at the third graph in Fig 8.5, the n = 7 sine waves are folded into an n = 1 sine wave. In general, if n_h represents a frequency higher than the Nyquist frequency, then the signal or amplitude of that wave will be folded down to a frequency of $n = N - n_h$, where it will be added to any true amplitude that already exists at n.

Since this folding or reflection occurs around the Nyquist frequency, it is also known as the ***folding frequency***. Such folding is readily apparent when wave amplitudes are plotted as spectral energies (to be discussed in Section 8.6). As illustrated in Fig 8.6, any nonzero wave amplitudes and spectral energies in the "true" signal at frequencies higher than the Nyquist frequency are folded back and added to the energies of the "true" signal at the lower frequencies, yielding an aliased (and erroneous) spectrum.

Aliasing is a problem whenever two conditions both occur: (1) the sensor can respond to frequencies higher than the rate that the sensor is sampled; and (2) the true signal has frequencies higher than the sampling rate. As we already know, there is a spectrum of wavenumbers and frequencies of turbulence in the atmosphere, some of which are very high. All measurement systems have limitations on the rate at which they can sample.

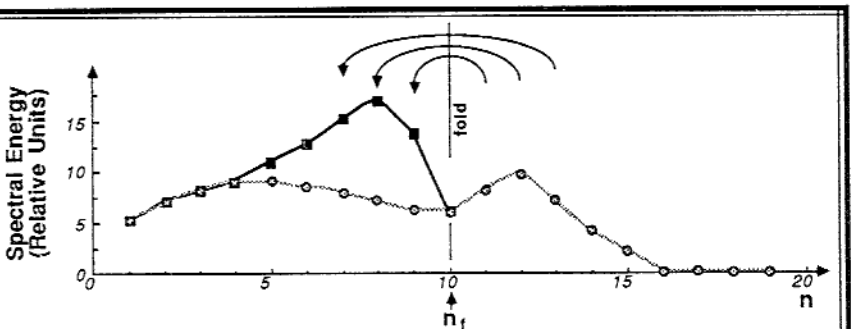

Fig. 8.6 Illustration that the "measured" spectrum (solid line) can give incorrect spectral energies as well as erroneous peak locations compared to the "true" spectrum (shaded line), when aliasing causes energies at the higher frequencies to fold back around the Nyquist frequency (n_f) and add to energies at the lower ones.

Sometimes this rate is given by limitations of the data logger or computer digitizer. If this is the case, then the raw electronic analog signal from the sensor (thermistor, thermocouple, gust probe accelerometer, etc) should be filtered by an analog electronic filter prior to the digitizing or sampling to remove frequencies higher than the Nyquist frequency. Sometimes the sensor itself has such a slow response that it performs the analog filtering automatically.

If the analog filtering is not performed, then there is no way to remove the erroneous aliased component from the resulting time series. Postprocessing of the discrete time series with digital filters will NOT work, because it is impossible to know what portion of the wave amplitude at the resolvable frequencies is real, and what is folded into it.

Digital averaging is sometimes successfully used for other reasons, however. Suppose that a sensor is designed with appropriate analog filters to yield unaliased data when sampled at a very high frequency. Next, suppose that the amount of this unbiased discrete data is too large to record in a convenient manner, or is coming in too fast to be processed. The stream of incoming discrete data values can be block averaged (e.g., average every 10 data points), or filtered with a variety of filters (e.g., Butterworth filters) before being recorded or processed further. This yields a lower-frequency sample without aliasing errors. If, however, one records only every fifth or tenth (or any interval) value from the sampled stream, then aliasing is again a problem.

Fourier analysis. Now that we are convinced that we can't resolve frequencies greater than the Nyquist frequency, why does the Fourier transform operation given by (8.4.1b) give amplitudes $F_A(n)$ up to the frequency $n = N - 1$? The answer is that it doesn't really. Looking at example 8.4.2 again, we again note that $F_q(n)$ for $n > n_f$ is just the complex conjugate of the $F_q(n)$ values for $n < n_f$. This is always the case and can be proved mathematically, assuming that the initial time series consists of only real numbers. Hence, the half of the $F_q(n)$ values for which $n > n_f$ give no new information.

Thus, the N different F_A values having both real and imaginary parts superficially gives 2N pieces of information, but since half of that is the complex conjugate of the other half, we are left with only N pieces of spectral information. It is reassuring that given only N data points in our original time series in physical space, we require only N pieces of information in phase space to precisely describe the data.

For an original time series consisting of complex numbers (2N pieces of data), the Fourier transform does not have the complex conjugate property described above, resulting in 2N pieces of information is phase space too. For meteorological data where the time series is usually real, we still need to utilize the whole Fourier transform with the complex conjugate information, because without it the inverse transform will produce complex numbers instead of our desired real number physical field.

Data Window. Fourier series apply to infinite-duration periodic data sets. Stated in other words, if we examine only a finite size record of data, the Fourier analysis implicitly assumes that the data is periodic and thus repeats itself both before and after our limited period of measurement.

In boundary layer meteorology, nothing is periodic for infinite time, or for infinite distance. Given a true signal (for example temperature) that varies as in Fig 8.7a, if we measure it over period $\mathbb{P}$ (our ***data window***) as in Fig 8.7b, then we are left with the segment shown in Fig 8.7c. Given this segment, the Fourier analysis assumes that it is dealing with a periodic (repeating) signal as shown in Fig 8.7d.

In this example, a smoothly varying meteorological signal appears as a saw-tooth pattern to the Fourier analysis. From basic calculus, recall that a Fourier analysis can indeed describe series such as sawtooth or square wave patterns, but a wide range of frequencies are required to get the sums of all the sines and cosines to make the sharp bends at the points of the teeth. These spurious frequencies are called ***red noise*** by analogy to visible light because they appear at the low frequency end of the spectrum. To avoid red noise, we must at the very least ***detrend*** the data series by subtracting the straight line best-fit from the data segment (Fig 8.7c), leaving a modified time series as exemplified in Fig 8.7e.

In general, any very low frequency that has a period longer than our whole sampling period will also generate the noise. If we know a-priori the period of this frequency, such as diurnal or annual, then we can perform a least-squares fit of this frequency to the time series and subtract the result from the series. Otherwise, we might try to fit a simple polynomial curve to the data and subtract it to both detrend it and remove these low frequencies.

Even after detrending, the sharp edges of the data window cause what is known as ***leakage***, where spectral estimates from any one frequency are contaminated with some spectral amplitude leaking in from neighboring frequencies. To reduce leakage, a modified data window with smoother edges is recommended, such as is shown in Fig 8.7f. Although a variety of smoothers can be used, a common one utilizes sine or cosine squared terms near the beginning and ending 10% of the period of record, and is known as a ***bell taper***:

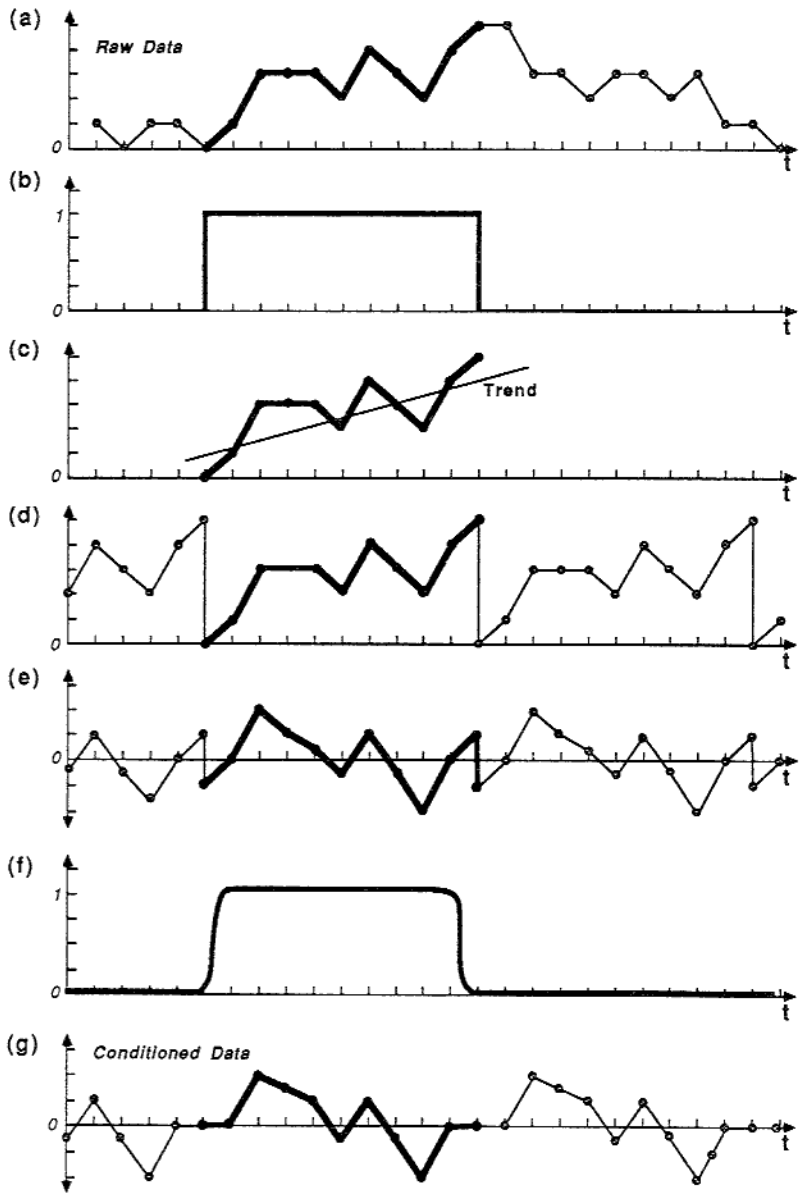

Fig. 8.7 A true signal (a) sampled over a finite time (b) gives the segment (c) that is assumed to be periodic (d) by the Fourier transform. When the detrended signal (e) is sine or cosine tapered (f) the result is called "conditioned" data (g). This "conditioned" data (g) can then be used by FFT routines.

$$W(k) = \begin{cases} \sin^2(5\pi k/N) & \text{for } 0 \le k \le 0.1N \\ 1 & \text{elsewhere} \\ \sin^2(5\pi k/N) & \text{for } 0.9\,N \le k \le N \end{cases} \qquad (8.4.3)$$

When this window weight, W(k), is multiplied by the time series, A(k), the result yields a modified time series with fluctuations that decrease in amplitude at the beginning and end of the series (see Fig 8.7g). The Fourier transform can then be performed in this modified time series.

The bell taper data window is not without its problems. Although the tapered ends reduced the leakage, they also reduce our ability to resolve spectral amplitude differences between small changes in frequencies. Also, the tapered window reduces high-frequency noise at the expense of introducing low-frequency noise.

The process of detrending, despiking (removing erroneous data points), filtering, and bell tapering is known as ***conditioning*** the data. Conditioning should be used with caution, because anytime data is modified, errors or biases can be introduced. The best recommendation is to do as little conditioning as is necessary based on data quality.

8.5 Fast Fourier Transform

The fast Fourier transform, or ***FFT***, is nothing more than a discrete Fourier transform that has been factored and restructured to take advantage of the binary computation processes of the digital computer. As a result, it produces the same output, and has the same limitations and requirements as the discrete transform. It can also be used for forward as well as inverse transforms. The description that follows is not meant to be a comprehensive review of FFT methods, but is designed to give an overview of the process.

In general, both the forward and the inverse discrete transform can be written as

$$X = \sum_{\substack{k=0 \text{ (forward)} \\ n=0 \text{ (inverse)}}}^{N-1} Y\,Z^{nk} \qquad (8.5a)$$

where

Forward Transform	Inverse Transform
$X(n) = F_A(n)$	$X(k) = A(k)$
$Y(k) = A(k)/N$	$Y(n) = F_A(n)$
$Z_N = \exp(-i2\pi/N)$	$Z_N = \exp(i2\pi/N)$

The decimal numbers n and k can be represented by their binary equivalents:

$$n = \sum_{j=0}^{\infty} 2^j n_j \qquad \text{and} \qquad k = \sum_{j=0}^{\infty} 2^j k_j \tag{8.5b}$$

where n_j and k_j represent the individual bits of the number. For example, if N = 8, then we need only three bits (j = 0 to 2) to represent n and k, since they can take on values of only 0 to 7. Thus $n = 4 \cdot n_2 + 2 \cdot n_1 + 1 \cdot n_0$. For example, 101 is the binary representation of the decimal 5, giving $n_2 = 1$, $n_1 = 0$, and $n_0 = 1$.

Using this binary representation, any function of n is now a function of n_2, n_1, and n_0, with similar forms for functions of k. Thus, X(n) becomes $X(n_2, n_1, n_0)$. Equation (8.5a) can now be rewritten, using the forward transform with N = 8 as the example, as:

$$X(n_2, n_1, n_0) = \sum_{k_2=0}^{1} \sum_{k_1=0}^{1} \sum_{k_o=0}^{1} Y(k_2, k_1, k_0)\, Z^{(4n_2 + 2n_1 + n_o)(4k_2 + 2k_1 + k_o)}$$

Performing the multiplications in the exponent of Z, rearranging terms, and remembering that Z to certain powers equals unity because of the nature of sines and cosines, we find:

$$X(n_2, n_1, n_0) = \sum_{k_o=0}^{1} \sum_{k_1=0}^{1} \sum_{k_2=0}^{1} Y(k_2, k_1, k_0)\, Z^{4n_0k_2} Z^{4n_1k_1} Z^{2n_ok_1} Z^{4n_2k_o} Z^{2n_1k_o} Z^{n_ok_o}$$

In this last equation the Z's are essentially weighting factors. To solve this equation, the inner sum is performed, using only the first weight because it is the only weight that is a function of k_2. When the next sum is performed, the additional two weights are included. Finally, the last sum uses the remaining three weights. This pattern of solving the sums, and gradually eliminating the k bits and replacing them with n bits can be programmed recursively, requires relatively little scratch storage, and is very efficient in computer time.

To a first approximation, the normal discrete Fourier transform requires N^2 operations, while the FFT requires only $(3N/2)\log_2 N$ operations. For small data sets ($N < 100$) the resulting computer time or cost difference is insignificant for all practical purposes, because of other overhead costs such as input and output. But for a data set of 1000 points, for example, the FFT computation takes 0.5% of the time that a traditional discrete transform computation would take. There is even some microprocessor hardware available that is specially configured to run FFTs. The bottom line is that the FFT is fast.

Most modern computer centers, and some statistical packages for microcomputers,

have "canned" FFT algorithms that users can access without having to write their own. Some of the early FFT packages were restricted to data sets with $N = 2^m$, where m was any integer. This meant that data sets slightly too long were truncated to the proper size, or data sets slightly too short we lengthened by adding bogus data (often zeros or the mean value). Both of these data mutilation tricks are not recommended. Modern FFTs factor the series into a variety of prime numbers in addition to the prime number 2, resulting in very little truncation of the time series.

One problem with all discrete Fourier transforms including FFTs, is that the input must consist of equally-spaced data points. No missing data is allowed. If the data set has gaps caused by instrument failures or by spurious data spikes that were removed, then artificial data points must be inserted to fill the gap. One is not allowed simply to close the gap by bringing the remaining parts of the data set together, because this alters the periods or wavelengths present in the original signal. The artificial data points must be chosen with care, otherwise this "fudge" can destroy an otherwise unbiased data set. Data with significant gaps can be analyzed with periodogram methods instead (see Section 8.9).

8.6 Energy Spectrum

8.6.1 Discrete Energy Spectrum

In meteorology we are frequently curious about how much of the variance of a time series is associated with a particular frequency, without regard to the precise phase of the waves. Indeed for turbulence, we anticipate that the original signal is not physically like waves at all, but we still find it useful to break the signal into components of different frequencies that we like to associate with different eddy sizes.

The square of the norm of the complex Fourier transform for any frequency n is:

$$|F_A(n)|^2 = [F_{\text{real part}}(n)]^2 + [F_{\text{imag. part}}(n)]^2 \qquad (8.6.1a)$$

When $|F_A(n)|^2$ is summed over frequencies n = 1 to N-1, the result equals the total biased variance of the original time series:

$$\sigma_A^2 = \frac{1}{N}\sum_{k=0}^{N-1}(A_k - \overline{A})^2 = \sum_{n=1}^{N-1}|F_A(n)|^2 \qquad (8.6.1b)$$

Thus, we can interpret $|F_A(n)|^2$ as the portion of variance explained by waves of frequency n. Notice that the sum over frequencies does not include n=0, because $|F_A(0)|$ is the mean value and does not contribute any information about the variation of the signal about the mean. To simplify the notation for later use, define: $G_A(n) = |F_A(n)|^2$. The ratio $G_A(n) / \sigma_A^2$ represents the fraction of variance explained by component n, and is

very much like the correlation coefficient squared, r^2.

For frequencies greater than the Nyquist frequency the $|F_A(n)|^2$ values are identically equal to those at the corresponding folded lower frequencies, because the Fourier transforms of high frequencies are the same as those for the low frequencies, except for a sign change in front of the imaginary part. Also, since frequencies higher than the Nyquist cannot be resolved anyway, the $|F_A(n)|^2$ values at high frequencies should be folded back and added to those at the lower frequencies.

Thus, ***discrete spectral intensity (or energy)***, $E_A(n)$, is defined as $E_A(n) = 2 \cdot |F_A(n)|^2$, for n = 1 to n_f, with N = odd. For N = even, $E_A(n) = 2 \cdot |F_A(n)|^2$ is used for frequencies from n = 1 to $(n_f - 1)$, along with $E_A(n) = |F_A(n)|^2$ (not times 2) at the Nyquist frequency. This presentation is called the ***discrete variance (or energy) spectrum***. It can be used for any variable such as temperature, velocity, or humidity to separate the total variance into the components, $E_A(n)$, related to different frequencies. For variables such as temperature and humidity, however, we must not associate the resulting spectrum with concepts of eddy motions, because variations in these variables can persist in the atmosphere in nonturbulent flow as the "footprints" of formerly active turbulence.

The variance of velocity fluctuations, u', has the same units as turbulence kinetic energy per unit mass. Thus, the spectrum of velocity is called the ***discrete energy spectrum***. As defined above, the name "energy spectrum" is sometimes used for all variance spectra.

8.6.2 Spectral Density

Although this chapter has dealt with discrete spectra, a number of theoretical concepts such as the spectral similarity discussed in the next chapter use continuous spectral representations. Namely, instead of summing the discrete spectral energy over all n to yield the total variance, these theories assume that there is a ***spectral energy density***, $S_A(n)$ that can be integrated over n to yield the total variance.

$$\sigma_A^2 = \int_n S_A(n)\, dn \qquad (8.6.2a)$$

The spectral energy density has units of A squared per unit frequency.

We can approximate the spectral energy density by

$$S_A(n) = \frac{E_A(n)}{\Delta n} \qquad (8.6.2b)$$

where Δn is the difference between neighboring frequencies. When n is used to represent frequency, $\Delta n = 1$. For other representations of frequency such as f, we will find that Δf is not necessarily equal to unity.

The $S_A(n)$ points estimated from (8.6.2b) can then be connected with a smooth curve to represent the shape of the spectrum. An example of this was shown in Chapter 2, Fig. 2.2. Thus, even with discrete meteorological data, we can estimate spectral densities that can be compared to theories.

8.6.3 Example

Problem: Use the results from the N = 8 data point example of section 8.4.2 to calculate the discrete spectral energies for all frequencies. Plot the result in the usual presentation format for discrete spectra. Show an additional graph of the estimate of spectral density.

Solution:

n	$F_q(n)$	$\lvert F_q(n)\rvert^2$	$E_q(n)$	$S_q(n)$
0	7.0 (= mean)			
1	0.28 - 1.03 i	1.14	2.28	2.28
2	0.5	0.25	0.5	0.5
3	-0.78 - 0.03 i	0.61	1.22	1.22
$4 = n_f$	1.0	1.0	1.0	1.0
5	-0.78 + 0.03 i	0.61		
6	0.5	0.25		
7	0.28 + 1.03 i	1.14		
	Sum =	5.0 =	5.0	

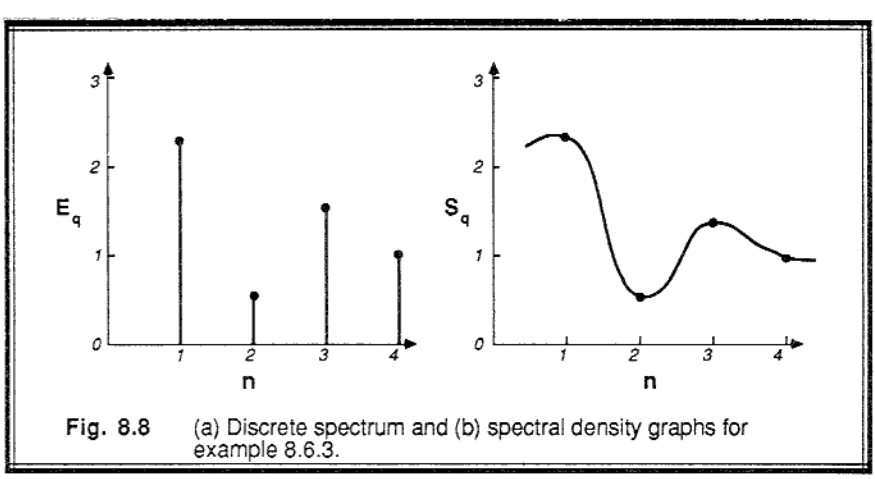

Fig. 8.8 (a) Discrete spectrum and (b) spectral density graphs for example 8.6.3.

where $E_q(n)$ has units of specific humidity squared, and $S_q(n)$ has units of specific humidity squared per unit frequency. Finally, the discrete spectrum is plotted in Fig 8.8a, and the spectral energy density is plotted in Fig 8.8b.

Discussion. The sum of the spectral energies equals the biased variance of the original signal, $\sigma_q^2 = 5.0$. This is always a good check of the FFT for you to perform.

8.6.4 Graphical Presentation of Atmospheric Spectra

A wide range of intensities are present in atmospheric turbulence spectra over an even larger range of frequencies. Atmospheric turbulence spectral energies characteristically peak at the lowest frequencies, namely at about 1 to 10 cycles per hour. At higher frequencies, the spectral energy decreases. For example, at frequencies of 10^4 cycles per hour the energy is one to two orders of magnitude smaller than at the peak.

We are often concerned about the full range of the spectrum: the peak is associated with the production of turbulence and usually the largest eddy sizes; the middle frequencies are associated with the inertial subrange, which is important for estimated dissipation rates; and the highest frequencies are associated with the dissipation of TKE into heat by viscous effects. Hence, we need a way to graphically present the spectral data in a form that not only highlights the important peaks and other characteristics, but which shows all portions of the wide range of data.

In the discussions that follow, a single idealized spectrum is presented in a variety of formats in Fig 8.9. The data for these plots is listed in Table 8-1. See Chapter 9 for examples of real atmospheric spectra.

Linear-linear presentation. When $S_A(f)$ is plotted vs. f on a linear-linear graph, the result has the desirable characteristic that the area under the curve between any pair of frequencies is proportional to the portion of variance explained by that range of frequencies. Unfortunately, the plot is useless to view because the wide range in values results in a compression of the data onto the coordinate axes (see Fig 8.9a). Alternatives include expanding the low frequency portion of the spectrum (Fig 8.9b) and plotting $f \cdot S(f)$ instead of just S(f) on the ordinate (Fig 8.9c). Both techniques focus on the spectral peak at the expense of losing information at the higher frequencies.

Note that the $f \cdot S(f)$ plot causes the apparent peak to shift from the low frequency end of the spectrum towards the middle of the spectrum. Since $f \cdot S(f)$ is also used in a number of the other formats listed below, we should not be deceived into thinking that the middle frequencies are the ones with the most spectral energy.

Semi-log presentation. By plotting $f \cdot S_A(f)$ vs. log f, the low frequency portions of the spectra are expanded along the abscissa. Also, the ordinate for the high frequency portions are enhanced because the spectral density is multiplied by frequency (see Fig 8.9d). Another excellent quality is that the area under any portion of the curve continues to be proportional to the variance.

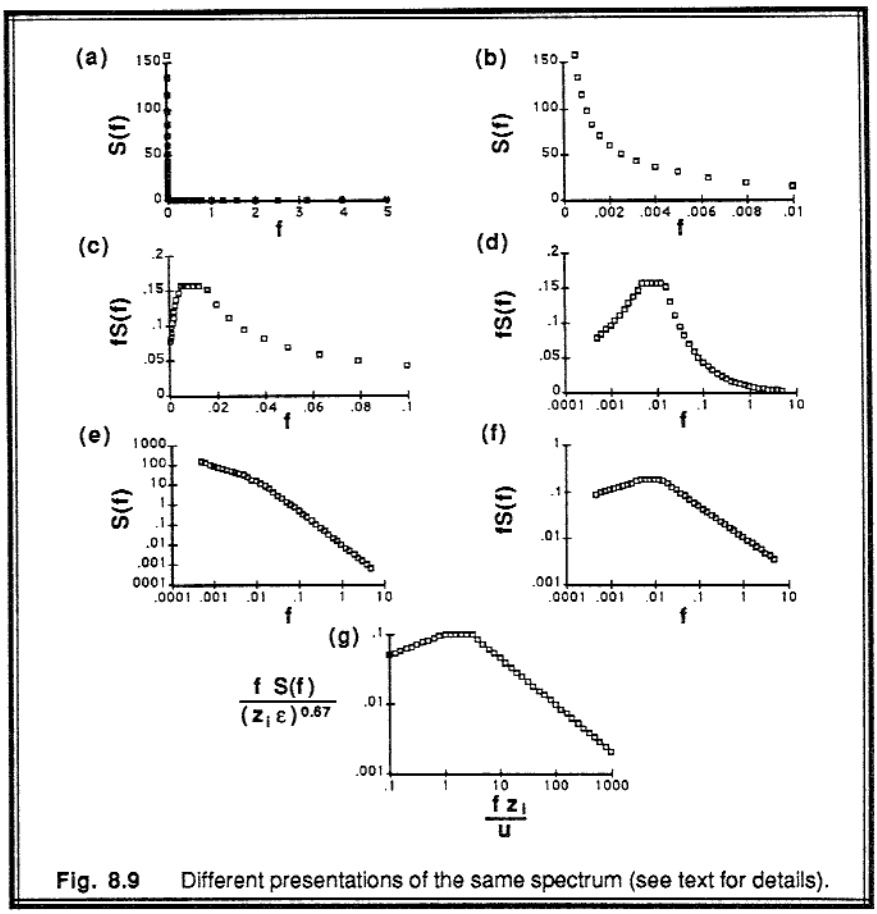

Fig. 8.9 Different presentations of the same spectrum (see text for details).

Log-log presentation. When $\log[S_A(f)]$ vs. $\log f$ is plotted, the result allows a wide range of frequencies and spectral densities to be displayed. Also, any power law relationships between $S_A(f)$ and f appear as straight lines on this graph. As will be discussed in more detail in the next chapter, $S_A(f)$ is proportional to $f^{-5/3}$ in the inertial subrange portion of the spectrum, which will appear as a straight line with -5/3 slope on a log-log graph (see Fig. 8.9e). Unfortunately, the area under the curve is no longer proportional to the variance.

Log f $S_A(f)$ vs. log f. A plot of $\log[f \cdot S_A(f)]$ vs. $\log f$, has all of the desirable characteristics of the log-log presentation described above. In addition, the quantity $f \cdot S_A(f)$ has the same units as the variance of A, making scaling or normalization easier. Unfortunately, the area under the curve is also not proportional to variance (see Fig. 8.9f). Regardless of this problem, this presentation is the most used in the literature.

Table 8-1. Artificial data and spreadsheet calculations used to demonstrate various ways to present spectra.

This is assumed to be the spectrum of a time series of velocity measurements.

Variable	Value
Zi (m)	1000
U (m/s)	5
Dissip.(m2 s-3)	0.002
Size	21

Logarithm of Normalized Frequency	Logarithm of Normalized Spectrum	Normalized Frequency	Normalized Spectrum	f (1/s)	S (m2/s3)	f S (m2/s2)
-1.0	-1.3010	0.1000	0.0500	0.0005	158.7401	0.0794
-0.8	-1.2412	0.1580	0.0574	0.0008	115.3005	0.0911
-0.6	-1.1807	0.2510	0.0660	0.0013	83.4309	0.1047
-0.4	-1.1204	0.3980	0.0758	0.0020	60.4486	0.1203
-0.2	-1.0602	0.6310	0.0871	0.0032	43.8016	0.1382
-0.0	-1.0000	1.0000	0.1000	0.0050	31.7480	0.1587
0.2	-1.0000	1.5850	0.1000	0.0079	20.0303	0.1587
0.4	-1.0000	2.5120	0.1000	0.0126	12.6385	0.1587
0.6	-1.0827	3.9810	0.0827	0.0199	6.5914	0.1312
0.8	-1.2175	6.3100	0.0606	0.0316	3.0495	0.0962
1.0	-1.3521	10.0000	0.0445	0.0500	1.4112	0.0706
1.2	-1.4868	15.8490	0.0326	0.0792	0.6530	0.0517
1.4	-1.6215	25.1190	0.0239	0.1256	0.3022	0.0379
1.6	-1.7562	39.8110	0.0175	0.1991	0.1398	0.0278
1.8	-1.8909	63.0960	0.0129	0.3155	0.0647	0.0204
2.0	-2.0255	100.0000	0.0094	0.5000	0.0299	0.0150
2.2	-2.1602	158.4890	0.0069	0.7924	0.0139	0.0110
2.4	-2.2949	251.1890	0.0051	1.2559	0.0064	0.0080
2.6	-2.4296	398.1070	0.0037	1.9905	0.0030	0.0059
2.8	-2.5643	630.9570	0.0027	3.1548	0.0014	0.0043
3.0	-2.6990	1000.0000	0.0020	5.0000	0.0006	0.0032

As will be discussed in the next chapter, both the abscissa and ordinate are often made dimensionless by normalizing with respect to scaling variables (see Fig 8.9g). The scaling variables used in this example are listed in Table 8-1.

8.7 Spectral Characteristics

Instead of discussing spectral behavior theoretically, this section demonstrates spectral behavior for a single variable through a series of examples with synthetic data. In each of the following cases, an artificial time series of 20 data points is plotted, along with the spectrum computed with an FFT program. The spectrum shows E(n) normalized by the total biased variance, and shows the fraction of the total variance explained by each frequency. The Nyquist frequency is n=10 for all cases.

Case A (Fig 8.10a): Simple waves of one frequency. All of these examples show a wave having four cycles per time period. The first four examples in this case show that the spectrum is independent of the phase of the original time series. A single simple wave in physical space produces a single spike in the spectrum at n=4 that explains all the variance. The fifth example shows that if the spectrum is normalized by the total variance, we still have a single spike that explains 100% of the variance. If the spectrum had not been normalized, the spike for this fifth case would have been twice as large as the spikes for the other four cases, because the time series for the fifth case consisted of a wave with twice the amplitude.

Case B (Fig 8.10b): Simple waves of different frequencies. The first example shows a time series filled by one wave, resulting in a spectrum with a spike at n = 1. The next three examples show waves with 4, 8, and 10 cycles per period in the time series, resulting in spectra with frequency spikes at n = 4, 8, and 10 respectively. The fifth example shows a time series with a wave having 12 cycles per period, but the aliasing problem causes this signal to be folded back to n = 8, where it appears as a spike on the spectrum.

Case C (Fig 8.10c): Frequencies between resolvable frequencies. The FFT consists of waves of the fundamental frequency (n = 1) and only the exact harmonics (n = 2, 3, 4,...). But what happens if the real signal has a frequency of n = 4.2 or 4.5? These examples show that a wave of n = 4.5 appears as two large spikes at n = 4 and n = 5. The closer the signal is to an exact harmonic, the greater the spectral energy at that harmonic and the smaller the energy at the next nearest neighbor. Notice that for a signal with n = 4.5, the spectrum not only has the two large spikes described above, but there is also a leakage of some small amount of spectral energy to all the other frequencies. We might expect that a real turbulence signal consisting of a multitude of frequencies, many of which are not exact harmonics of the fundamental frequency, will result in a spectrum with a lot of leakage, making it difficult to separate the true signals from the underlying noise.

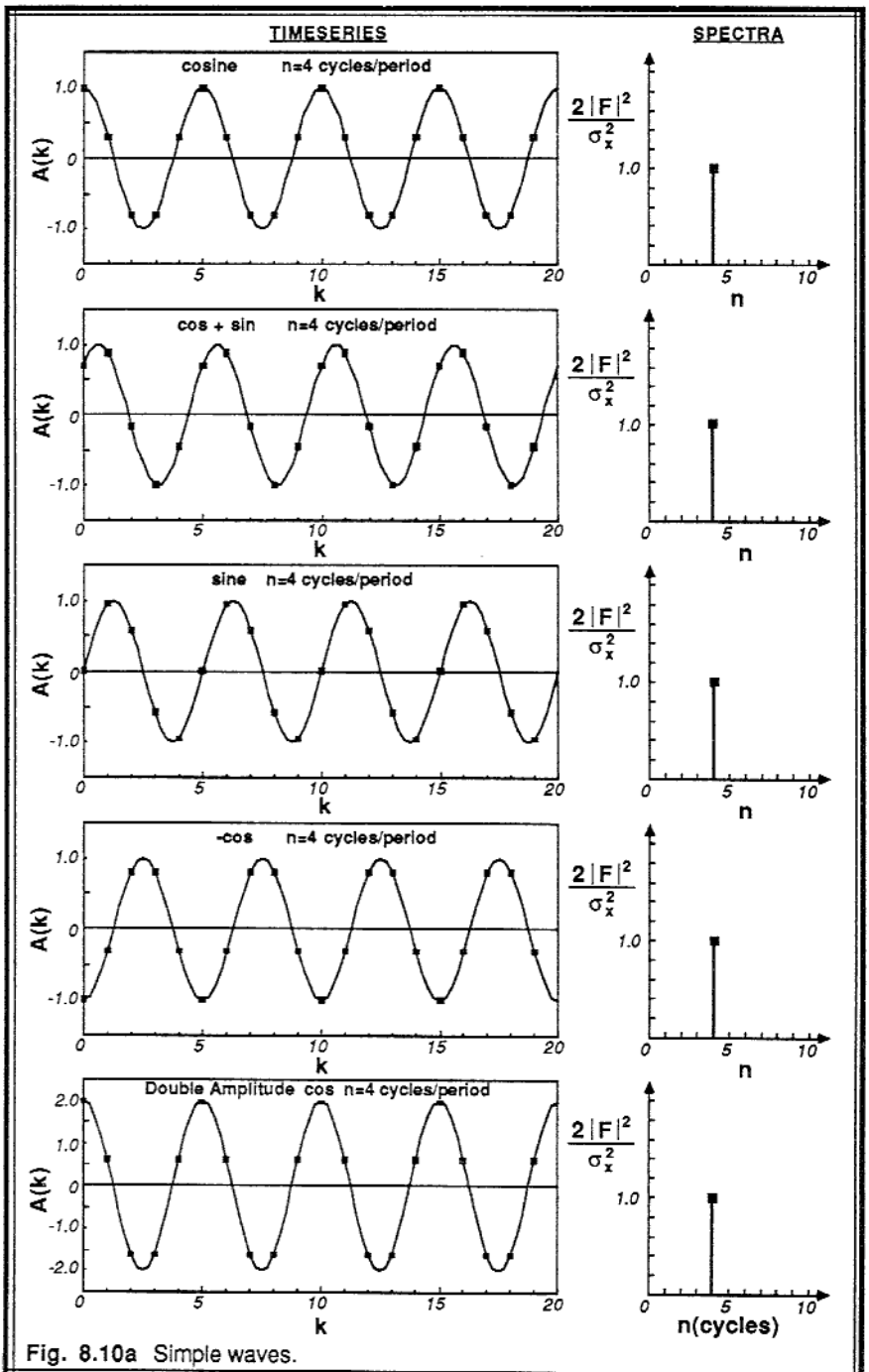

Fig. 8.10a Simple waves.

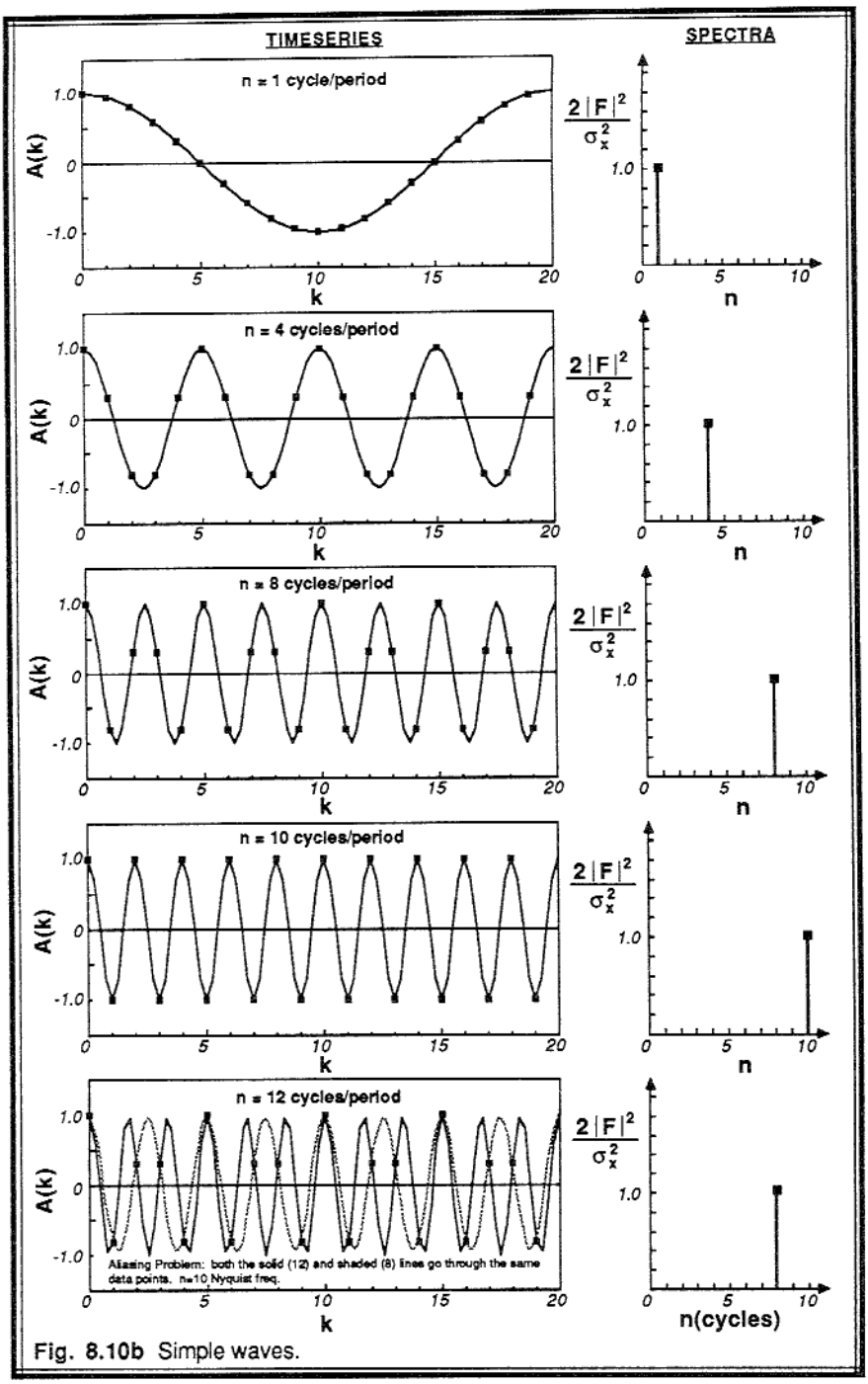

Fig. 8.10b Simple waves.

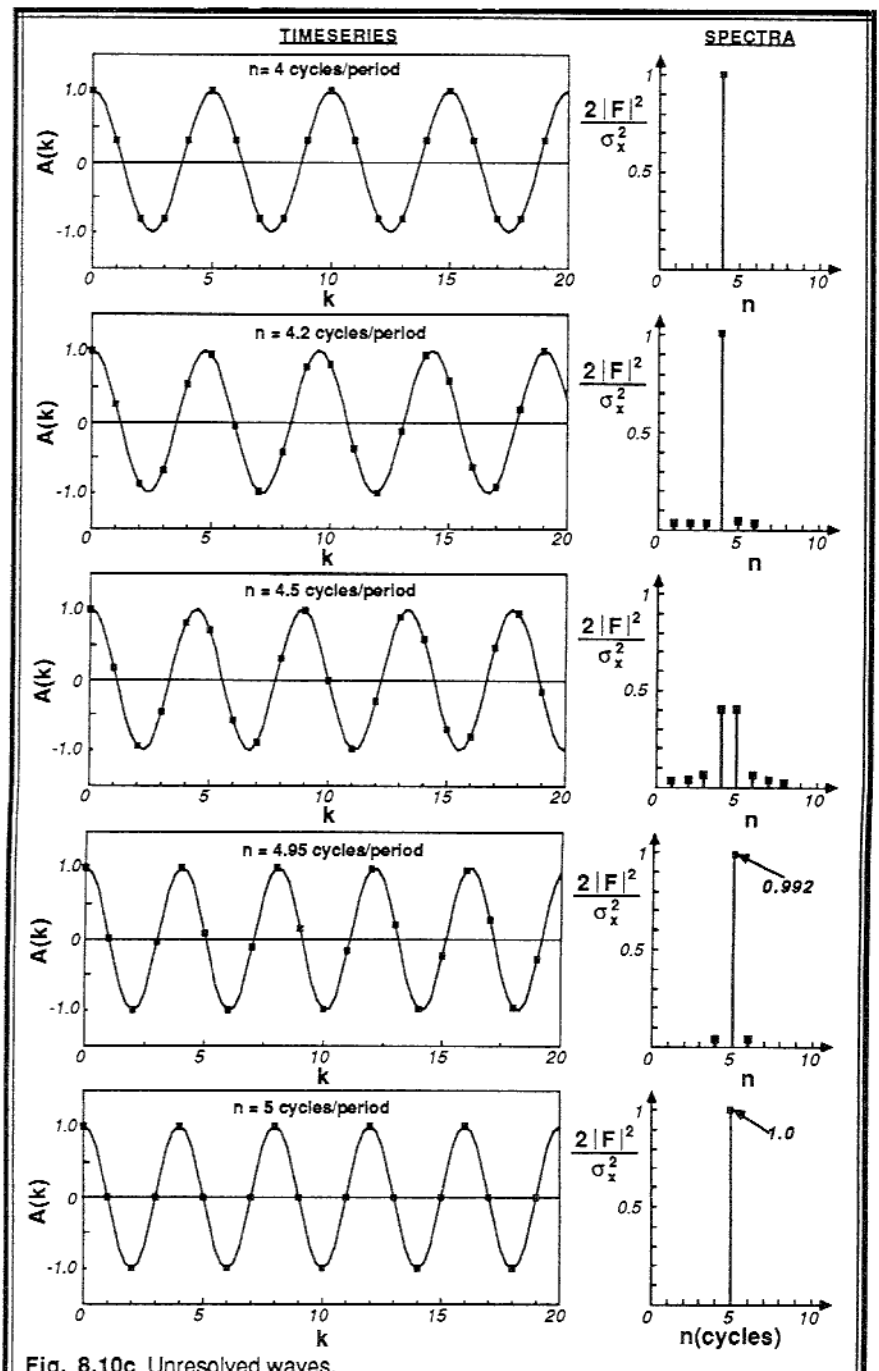

Fig. 8.10c Unresolved waves.

Case D (Fig 8.10d): Unresolvable high and low frequencies. The first example shows that if the real signal has n = 0.5, then the computed spectrum has a spike at n = 1 with a significant amount of leakage to higher frequencies. This is called ***red noise*** and will be discussed in Case E. At n = 1.5, there is still significant red noise. It is as if the leakage from the left side of the spike is folded back around n = 0 to larger n values. At n = 8.5, the leakage off the right of the peak appears to fold back to the left, creating a ***blue noise*** signal.

Case E (Fig 8.10e): Red noise. When signal with time period longer than the sampling period is truncated to fit within the sample window, the resulting periodic shape is fit by waves of the fundamental period and shorter. These waves are largest at the low-frequency end of the spectrum. As the wave period increases, this becomes more apparent. In the extreme case of a linear trend (which acts like an infinite period or wavelength wave), we find a purely red noise spectrum. Its name comes from the fact that the spectrum shows energy at the incorrect frequencies (i.e., error or noise), and that most of this noise is at the low frequencies (analogous to the red portion of the visible light spectrum). We see why it is important to detrend raw signals before computing the FFT.

Because of unresolvable low frequencies in general, and red noise in particular, most meteorologists do not consider frequencies of 3 or less as being reliable. Some use n=5 or n = 10 as the cut off. In any case, we look for at least three waves per sampling period before we are confident that the spectral results are telling us about the physics of the boundary layer. Often, these low frequencies are not even plotted on spectra that are presented in the literature.

Case F (Fig 8.10f): Red, white, and blue noise. White noise consists of approximately equal amplitude spectral energies across the whole range of frequencies. This can be produced by a spike in the time series, or by completely random "hash" signal. If we could hear white noise (e.g., the audio analogy), it would sound like a hiss, like many leaves rustling or many waves breaking.

Blue noise is associated with larger spectral amplitudes at the higher frequencies. A constant signal, shown in the fourth example, consists of just a mean value (i.e., at n = 0), and hence has zero variance and no spectral energy. A square wave yields a spectrum with many peaks and zeros.

Case G (Fig 8.10g): Leakage. The shorter a signal lasts within a record, the more difficult it is to resolve it. Each of these examples shows a signal with five cycles per period. In the first example, the spectrum shows the desired spike at n = 5 with no energy at other frequencies. However, as the signal is cut shorter and shorter, the energy from the spike at n = 5 leaks more and more into the neighboring frequencies. In the last example with just one wave left in the time series, the spectrum shows a nearly Gaussian spread. Hence, even though certain signals in the time series may be evident to the eye, the FFT can have difficulty detecting it.

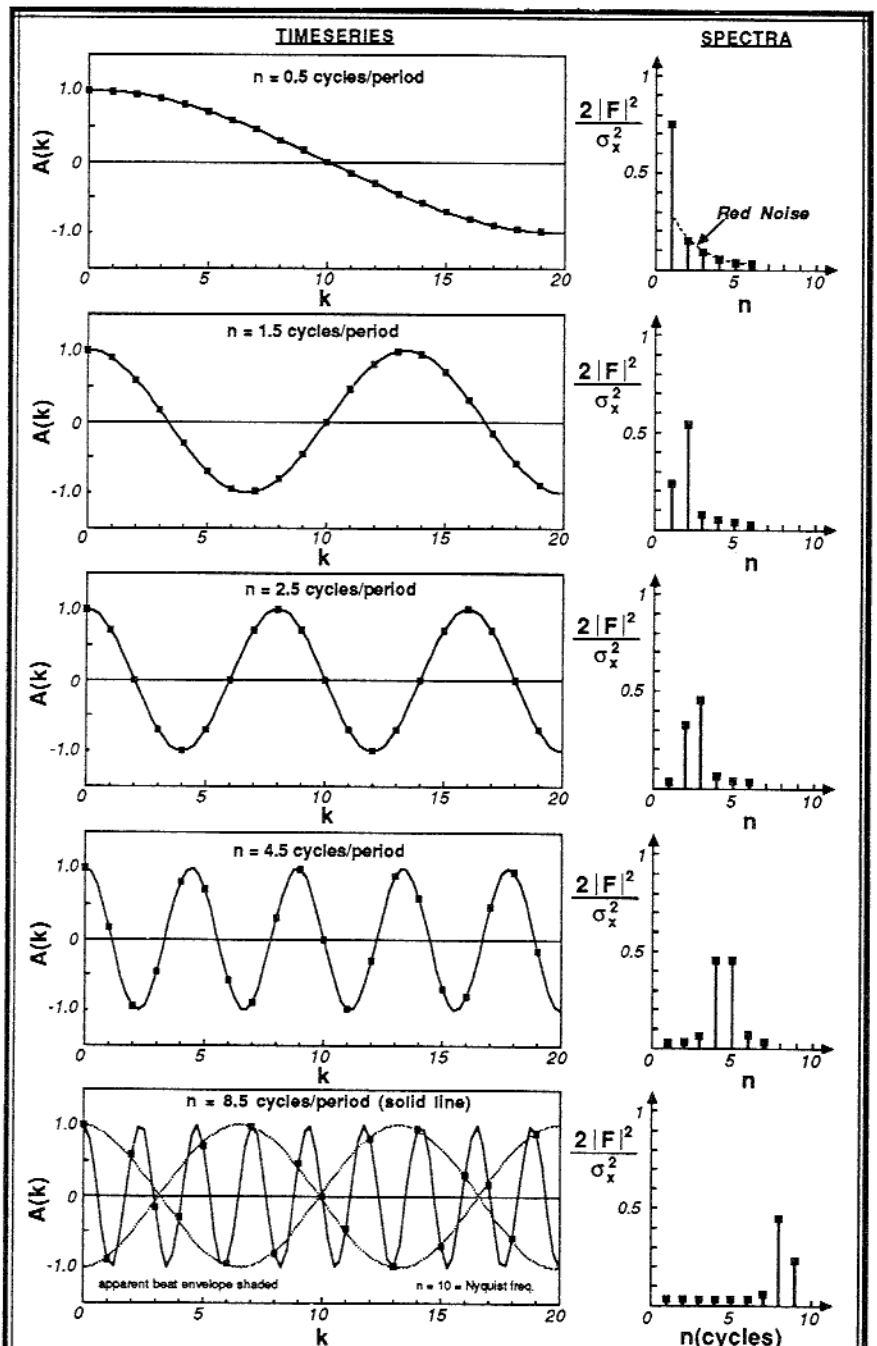

Fig. 8.10d Unresolved waves.

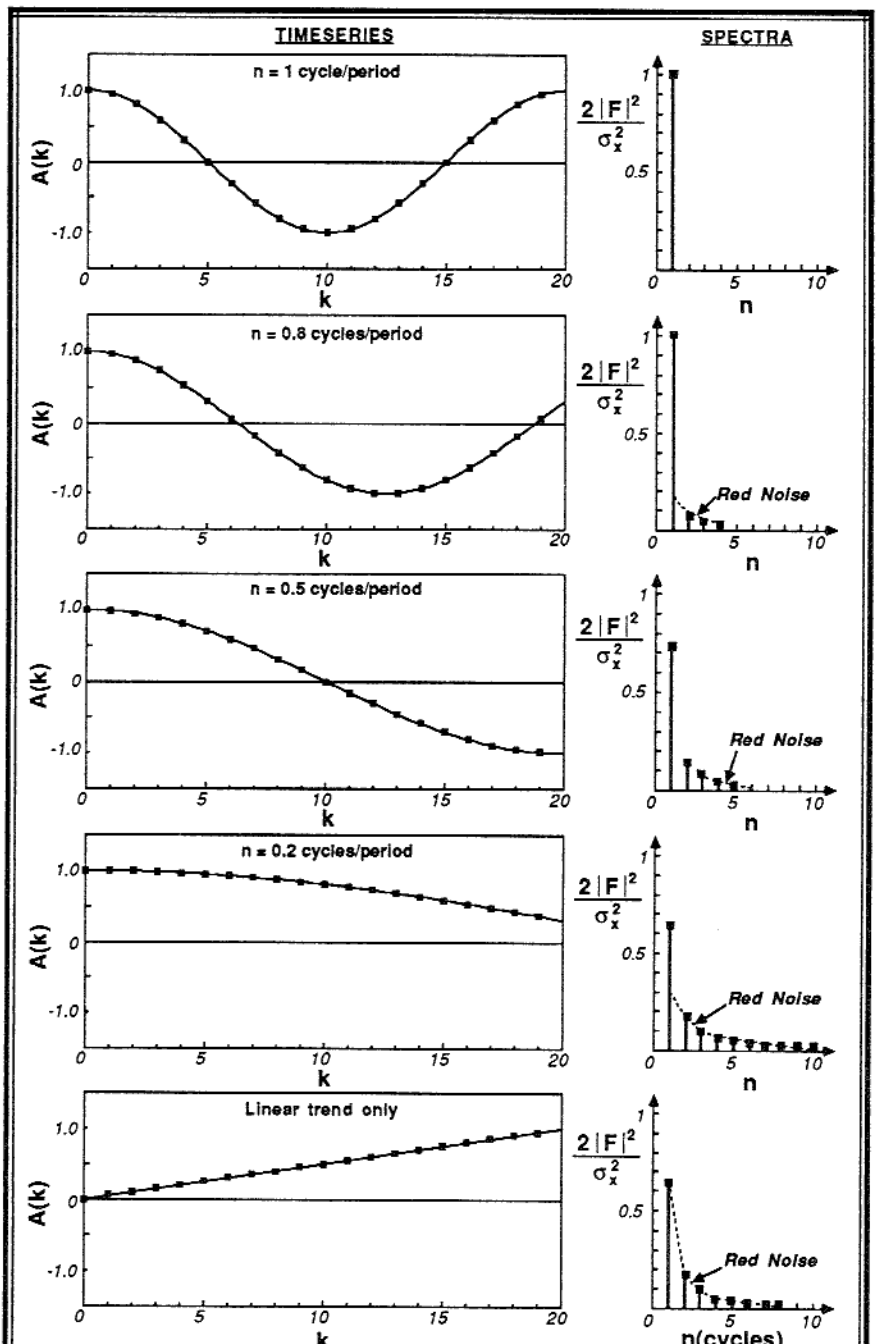

Fig. 8.10e Red noise.

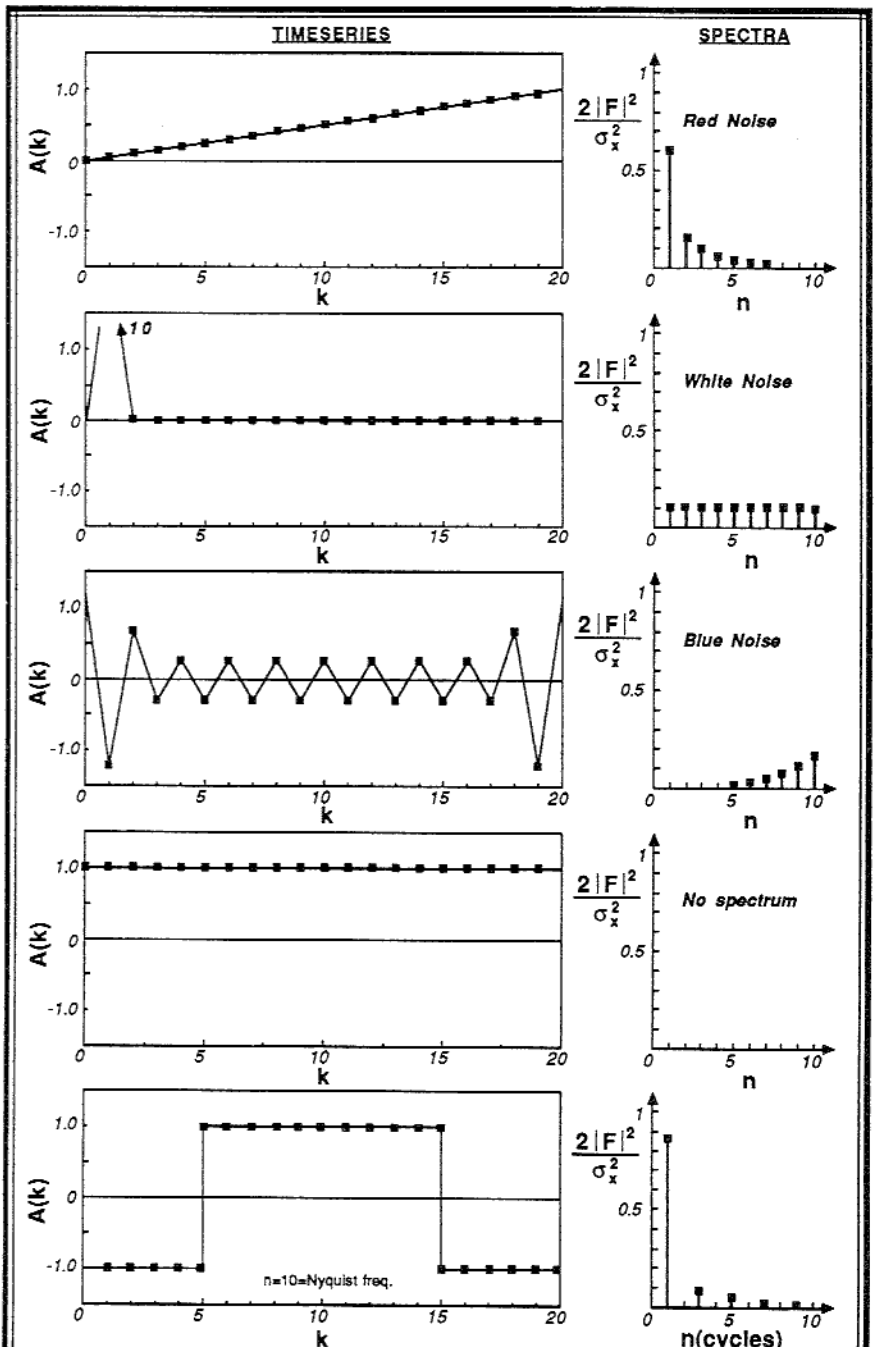

Fig. 8.10f Red, white and blue noise.

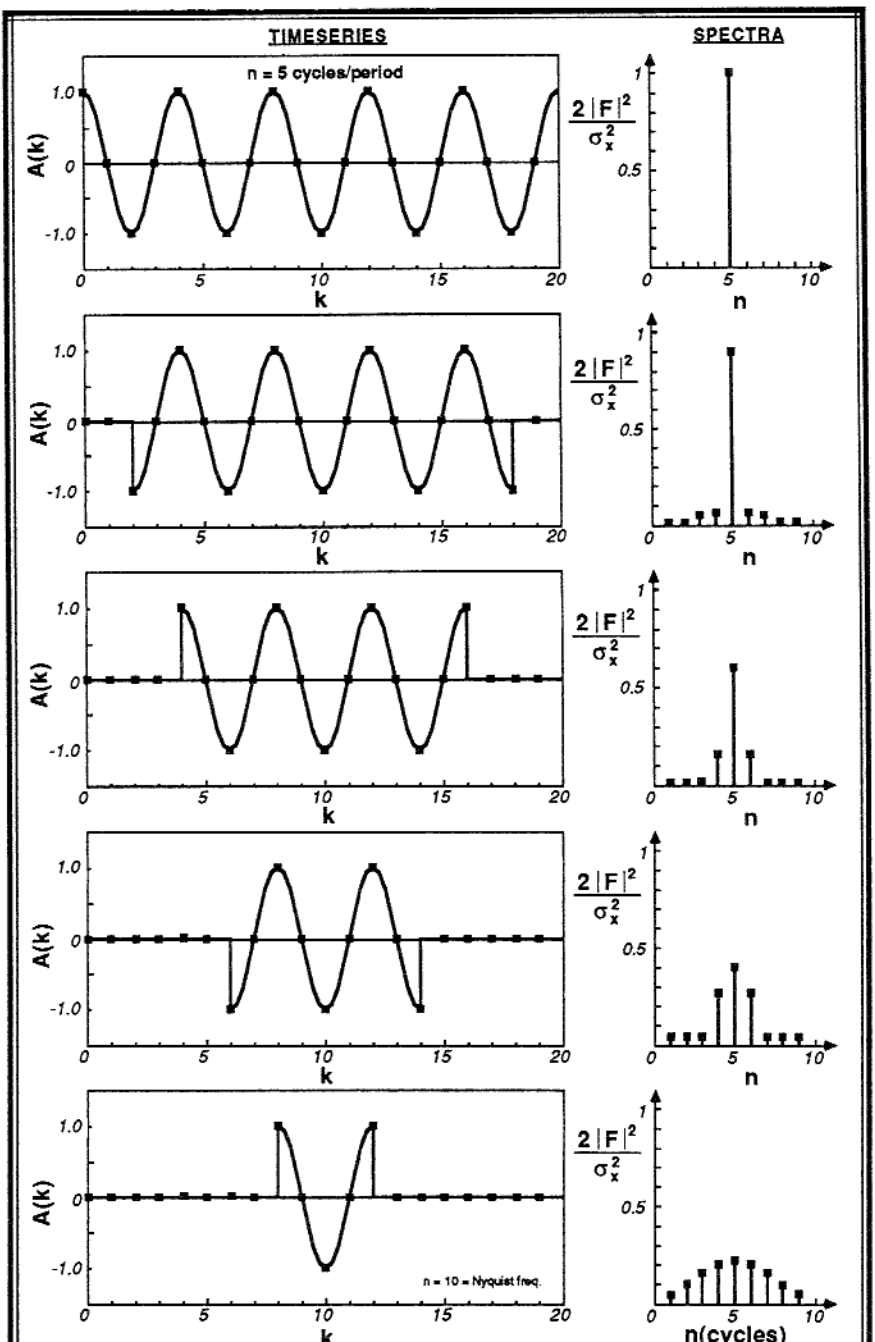

Fig. 8.10g Line broadening (leakage).

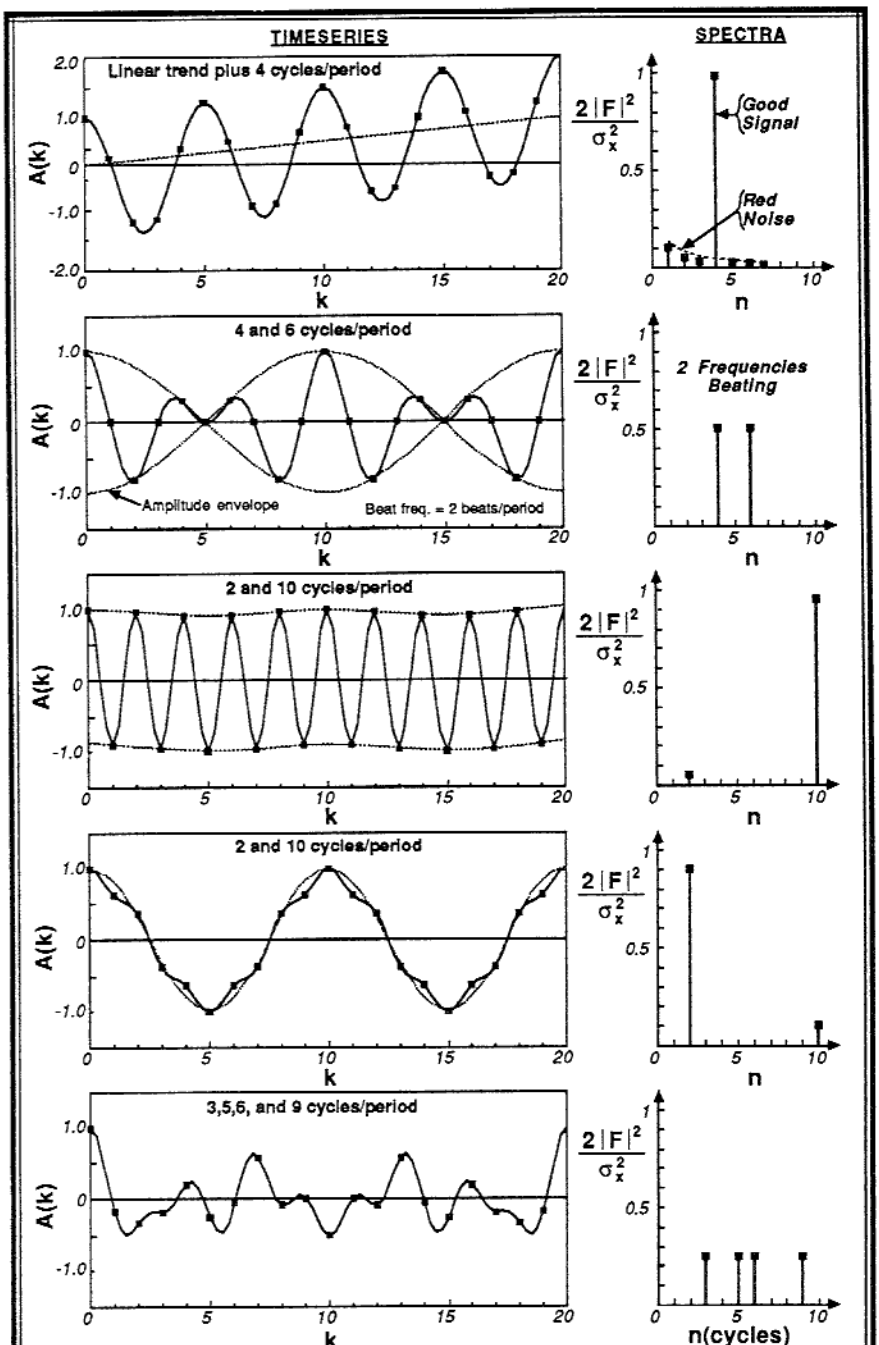

Fig. 8.10h Multiple waves.

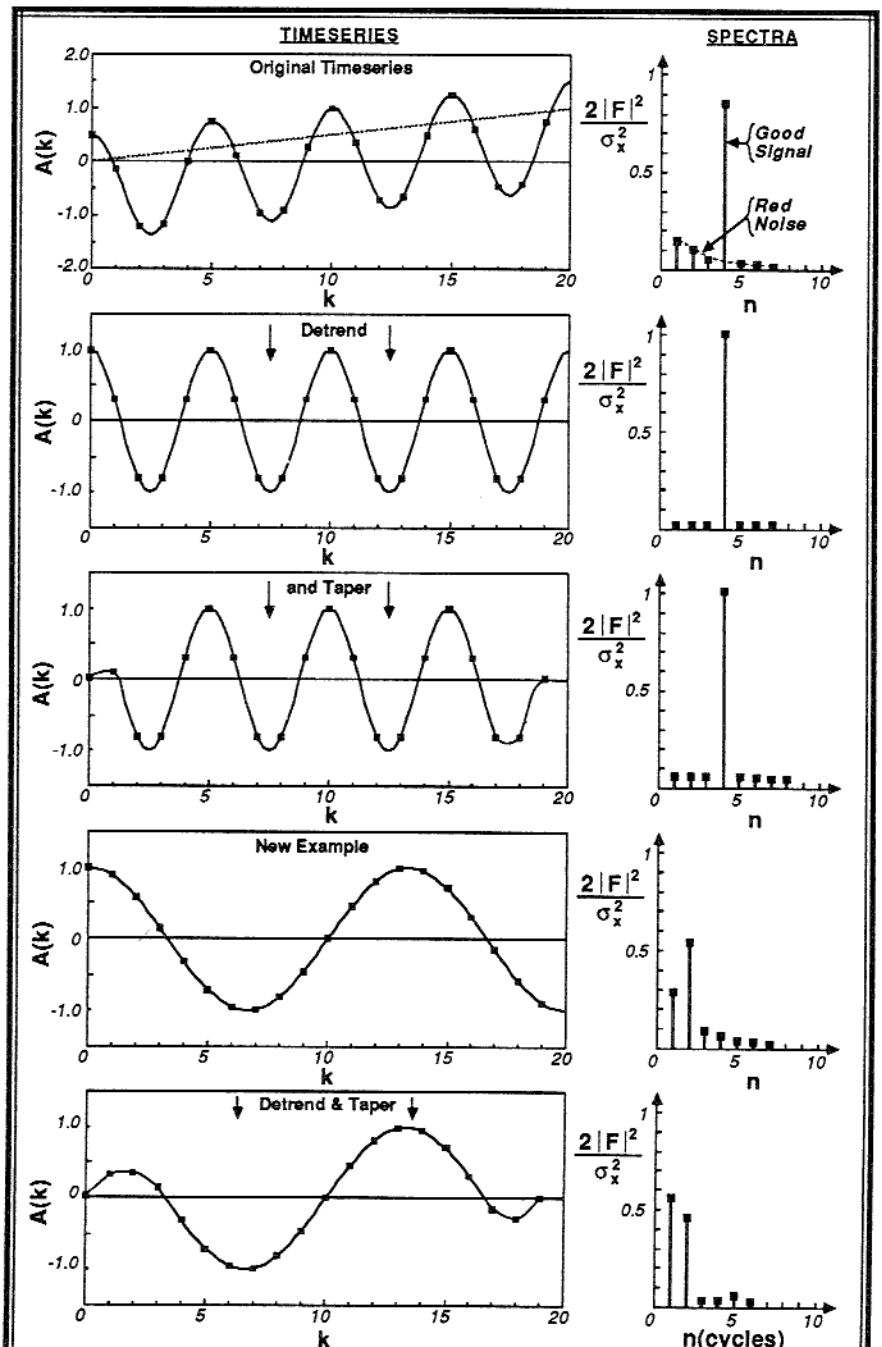

Fig. 8.10i Characteristics of DFT and FFT.

Case H (Fig 8.10h): Multiple Waves. These examples were constructed in reverse, where the spectrum was specified and the time series was generated with an inverse FFT. When the time series consists of the superposition of a number of different wave periods or wavelengths, the spectrum shows a number of spikes. If some of these waves are between harmonics or longer than the fundamental frequency, then the problems of spreading, leakage, and red noise are superimposed on the other resolvable signals. Also, for the second example, the two frequencies at n = 4 and 6 result in a beat frequency of 2, causing the amplitude envelope of the original time series to oscillate as shown.

Case I (Fig 8.10i): Conditioning. The first three examples show one situation of an original time series that is superimposed on a trend. Detrending the time series eliminates the red noise in the spectrum, and tapering the ends has little effect after that. The last two examples show a wave with n = 1.5, causing a significant amount of noise in the spectrum. However, after detrending and tapering, the spectrum yields the desired spikes at n = 1 and n = 2.

8.8 Spectra of Two Variables

Just as we can find the spectrum for a single variable, we can also find a spectrum for a product of two variables. For example, given observations of $w'(t)$ and $\theta'(t)$, we can create a new time series $w'\theta'(t)$ on which we can perform routine spectral analyses using an FFT. Occasionally it is useful to get more information about the spectrum of $w'\theta'$, such as how the phase of the w' fluctuations relate to the phase of the θ' fluctuations as a function of frequency. ***Cross-spectrum analysis*** relates the spectra of two variables.

8.8.1 Phase and Phase Shift

Phase refers to the position within one wave, such as at the crest or the trough (Fig 8.11a). It is often given as an angle. For example, the crest of a sine wave occurs at 90°, or at $\pi/2$ radians. ***Phase shift*** refers to the angle between one part of a wave like the crest and some reference point like a "start time" or the crest of another wave. For example, in Fig 8.11b the phase of the second wave is shifted 90° to the right of the first wave.

The equation for a single sine wave of amplitude C that is shifted by angle Φ to the right is:

$$A(k,n) = C(n)\cdot\sin\left(\frac{2\pi kn}{N} - \Phi(n)\right) \qquad (8.8.1a)$$

Through trigonometric identities, we can show that the same wave described above can also be written as the sum of one sine wave and one cosine wave:

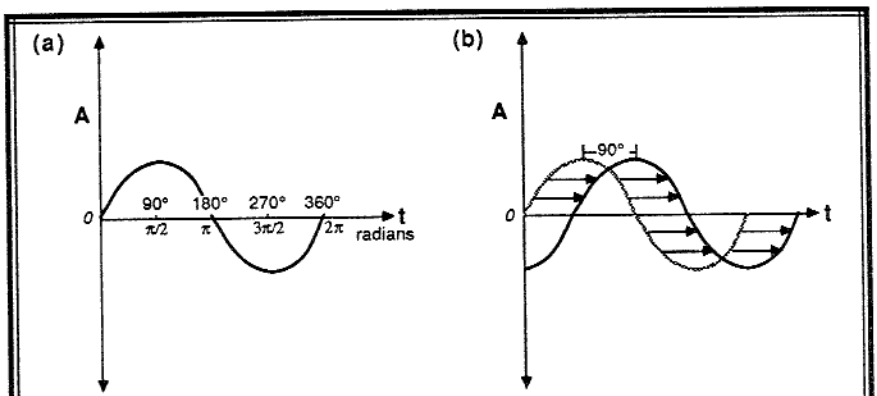

Fig. 8.11 (a) Phase angles and (b) example of a 90° phase shift.

$$A(k,n) = C_s(n)\cdot\sin\left(\frac{2\pi kn}{N}\right) + C_c(n)\cdot\cos\left(\frac{2\pi kn}{N}\right) \qquad (8.8.1b)$$

where $C_s = C\cdot\cos\Phi$ and $C_c = -C\cdot\sin\Phi$.

As shown in section 8.4.1 the Fourier transforms give the amplitudes of sine and cosine terms in the spectral decomposition of the original field. Thus, we can also interpret the spectra in terms of an amplitude and phase shift for waves of each frequency.

8.8.2 Cross Spectra

Define $G_A = |F_A(n)|^2$ as the unfolded spectral energy for variable A and frequency n. We can rewrite this definition as $G_A = F_A^*\cdot F_A$, where F_A^* is the complex conjugate of F_A, and where the dependence on n is still implied.

To demonstrate this last definition, let $F_A = F_{Ar} + i\cdot F_{Ai}$, where subscripts r and i denote real and imaginary parts respectively. Thus, the complex conjugate is simply $F_A^* = F_{Ar} - i\cdot F_{Ai}$. The expression for the spectral energy can now be written as:

$$\begin{aligned} G_A &= F_A^*\cdot F_A \\ &= (F_{Ar} - i\,F_{Ai})\cdot(F_{Ar} + i\,F_{Ai}) \\ &= F_{Ar}^2 + i\,F_{Ai}F_{Ar} - i\,F_{Ai}F_{Ar} - i^2F_{Ai}^2 \\ &= F_{Ar}^2 + F_{Ai}^2 \\ &= |F_A(n)|^2 \end{aligned}$$

leaving the magnitude squared as a real number.

Similarly, define the spectral intensity $G_B = F_B^* \cdot F_B$, for a different variable B. We can now define the ***cross spectrum*** between A and B by

$$G_{AB} = F_A^* \cdot F_B \qquad (8.8.2a)$$

$$= F_{Ar} F_{Br} + i F_{Ar} F_{Bi} - i F_{Ai} F_{Br} - i^2 F_{Ai} F_{Bi}$$

Upon collecting the real parts and the imaginary parts, the real part is defined as the ***cospectrum***, Co, and the imaginary part is called the ***quadrature spectrum***, Q:

$$G_{AB} = Co - i Q \qquad (8.8.2b)$$

where

$$Co = F_{Ar} F_{Br} + F_{Ai} F_{Bi} \qquad (8.8.2c)$$

and

$$Q = F_{Ai} F_{Br} - F_{Ar} F_{Bi} \qquad (8.8.2d)$$

Although not explicitly written in the equations above, F_A and F_B are functions of n, making both the cospectrum and quadrature spectrum functions of n too: Co(n) and Q(n).

The cospectrum is frequently used in meteorology, because the sum over frequency of all cospectral amplitudes, Co, equals the covariance between A and B, (i.e., $\sum_n Co(n) = \overline{a'b'}$). Note that the cospectrum computed as above is NOT equal to the spectrum of the time series of the product a'b'.

The quadrature spectrum is usually not used directly, but it too has a physical interpretation. The quadrature spectrum is equal to the spectrum of the product of b' times a phase shifted a', where a' is phase shifted a quarter period of n. In other words, the amount of time lag applied to a' depends on the frequency, n, such that the phase shift is always 90° for each n.

Three additional spectra can be constructed from the quad and co-spectra. An ***amplitude spectrum***, Am, can be defined as

$$Am = G_{AB}^* \cdot G_{AB}$$

$$= Q^2 + Co^2 \qquad (8.8.2e)$$

A large amplitude at any frequency n implies that A is very strongly correlated to B at that frequency, regardless of phase differences between A and B. In other words if both A and B have a strong amplitude component with frequency n = 5 even if A and B are out of phase, then Am will be large for n = 5. Also, if the amplitude is small for any frequency

n, then coherence and phase spectra (described next) are not significant (i.e., unreliable) for that frequency.

The ***coherence spectrum***, Coh, is defined by:

$$\mathrm{Coh}^2 = \frac{G^*_{AB}\, G_{AB}}{G_A\, G_B} = \frac{Q^2 + \mathrm{Co}^2}{G_A\, G_B} \qquad (8.8.2f)$$

This is essentially a normalized amplitude, and is a real number in the range 0 to 1. It acts very much like a frequency dependent correlation coefficient. Note that in some of the literature Coh^2 is defined as the coherence, rather than Coh. Like the amplitude spectrum, it is not a function of phase shift.

Finally, a ***phase spectrum***, Φ, can be defined as

$$\tan \Phi = Q / \mathrm{Co} \qquad (8.8.2g)$$

This can be interpreted as the phase difference between the two time series A and B that yielded the greatest correlation for any frequency, n. The phase spectrum can be used to infer the nature of the physical flow. For buoyancy waves, θ' is characteristically 90° out of phase with w'; while for turbulence, the two variables either in phase or 180° out of phase.

8.8.3 Example

Problem: Given the time series from section 8.4.2 for humidity, and the time series below for vertical velocity, w:

Index (k):	0	1	2	3	4	5	6	7
Time (UTC):	1200	1215	1230	1245	1300	1315	1330	1345
w (m/s):	0	-2	-1	1	-2	2	1	1

Find and plot:

a) the discrete Fourier transform and the spectrum for w
b) the cospectrum for w and q
c) the quadrature spectrum
d) the amplitude spectrum
e) the coherence spectrum
f) the phase spectrum.

Also find the discrete Fourier transform and the spectrum for the product w'q'.

Solution: The original time series are listed in Table 8-2 as a reference, along with the deviations squared and the series w'q'. The Fourier transforms for both w and q are

Table 8-2. Spectra and cospectra data, computed with an FFT program, and then displayed here in spreadsheet form.

Timeseries:

k	w	q	w'2	q'2	w'q'
0	0	8	0	1	0
1	-2	9	4	4	-4
2	-1	9	1	4	-2
3	1	6	1	1	-1
4	-2	10	4	9	-6
5	2	3	4	16	-8
6	1	5	1	4	-2
7	1	6	1	1	-1
Sum:	0	56	Sum: 16	40	Sum: -24
Mean:	0	7	Variance: 2	5	Covar: -3

Simple Spectra:

n	Fw real	Fw imag	Gw	Ew/$\overline{w'2}$	Fq real	Fq imag	Gq	Eq/$\overline{q'2}$
0	0.000	0.000			7.000	0.000		
1	-0.104	0.604	0.375	0.375	0.280	-1.030	1.140	0.456
2	-0.250	0.250	0.125	0.125	0.500	0.000	0.250	0.100
3	0.604	0.104	0.375	0.375	-0.780	-0.030	0.610	0.244
4	-0.500	0.000	0.250	0.125	1.000	0.000	1.000	0.200
5	0.604	-0.104	0.375		-0.780	0.030	0.610	
6	-0.250	-0.250	0.125		0.500	0.000	0.250	
7	-0.104	-0.604	0.375		0.280	1.030	1.140	
Sum:			2.000	1.000			5.000	1.000

Cross-spectra (based on F & G values above):

n	Gwq Co	Gwq Q	Am	Coh2	Phase(°)
0					
1	-0.651	0.062	0.428	1.000	174.52
2	-0.125	0.125	0.031	1.000	135.00
3	-0.474	-0.063	0.229	1.000	187.52
4	-0.500	0.000	0.250	1.000	180.00
5	-0.474	0.063	0.229	1.000	172.48
6	-0.125	-0.125	0.031	1.000	225.00
7	-0.651	-0.062	0.428	1.000	185.48
Sum:	-3.000	0.000			

Simple Spectrum of w'q' timeseries:

Fwq real	Fwq imag	Gwq	Ewq/$\overline{(w'q')'2}$
-3.000	0.000		
1.104	-0.354	1.343	0.398
-0.250	1.250	1.625	0.481
0.396	-0.354	0.282	0.084
0.500	0.000	0.250	0.037
0.396	0.354	0.282	
-0.250	-1.250	1.625	
1.104	0.354	1.343	
		6.750	1.000

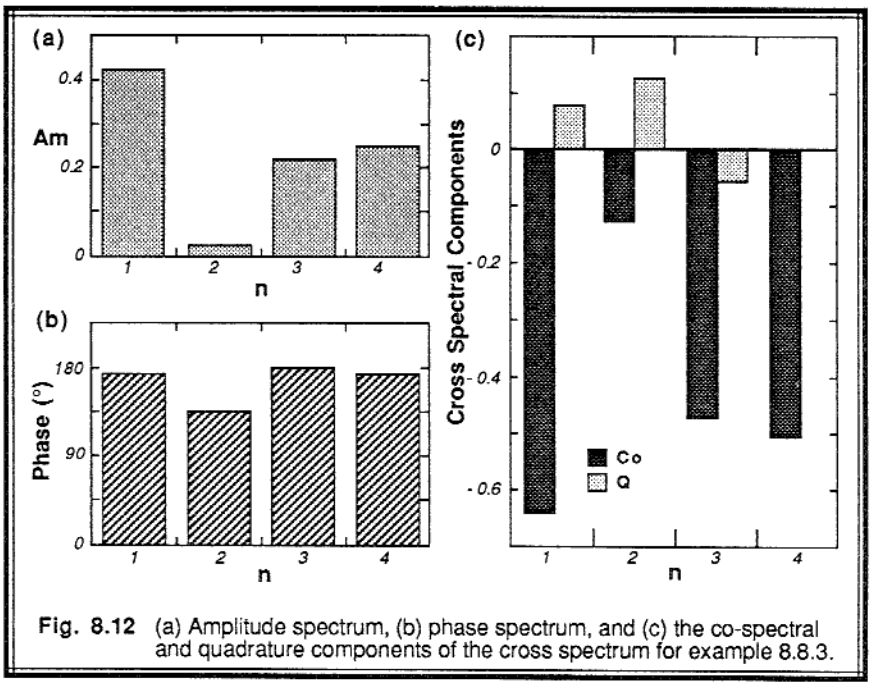

Fig. 8.12 (a) Amplitude spectrum, (b) phase spectrum, and (c) the co-spectral and quadrature components of the cross spectrum for example 8.8.3.

then found using an FFT program, and are listed in Table 8-2 along with their corresponding unfolded spectral intensities, G_w and G_q, and the fraction of variance explained, E_w/s_w^2 and E_q/s_q^2, where s^2 represents the variance.

Also listed is a subtable with co- and quad- spectral components of G_{wq}, the resulting values of Am, Coh^2, and the phase angles in degrees. These are plotted in Fig 8.12. Finally, the simple spectrum of the w'q' time series is listed.

Discussion: The biased variances of the w and q time series are 2.0 and 5.0, respectively. From Table 8-2, we see that the sum of the G_w and G_q spectral components equals their respective variances. This is always a good check to do with the analysis. The associated normalized spectral components, E_w/s_w^2 and E_q/s_q^2, sum to unity as desired. Also, the covariance $\overline{w'q'}$ = -3.0, which agrees with the sum of the Co cospectral components.

Looking at the original time series, we see that w' is usually positive when q' is negative, as confirmed by the negative covariance. Thus, we anticipate that w' and q' are 180° out of phase. The phase spectrum supports this. In fact, the only phase values which are substantially different from 180° are those for which the amplitude (Am) values are small, suggesting that these phase values can't be trusted.

It is surprising to find that the coherence is 1.0 for all frequencies. This indicates that there is a very close relationship between w and q for all frequencies or wavelengths, for this contrived example. For real turbulence data the coherence would not equal 1.0 for all frequencies.

Next, look at the individual q series. There is an obvious oscillation with three cycles within the whole period of record. In addition there is a background low frequency change of the time series. Looking at the simple spectrum for q, the spectral intensity is indeed large for n = 3 and n = 1. A similar conclusion can be reached for w. For both of these series, there is a distinct spectral minimum at n = 2.

This minimum shows up in the cospectrum at n = 2. Thus, waves with two cycles per period contribute little to the total covariance $\overline{w'q'}$. This is in sharp contrast with the w'q' time series itself, which shows a very definite n = 2 wave. The simple spectrum analysis of w'q' also yields the largest spectral component at n = 2. This tells us that the variance (not covariance) of the w'q' time series has a large contribution at n = 2, even though the covariance itself, $\overline{w'q'}$, has a minimum at n = 2.

In the discussion presented above, it was easy to compare the spectra with features in the original time series, because the series were so short. For real turbulence data consisting of thousands of data points, it is not so easy to pick out features by eye. For these situations, spectral analysis is particularly valuable.

8.9 Periodogram

The periodogram is just a least squares best fit of sine and cosine waves to the original signal (i.e., to the time series). Because the original time series need not consist of evenly spaced data points for the periodogram to work, it has a very distinct advantage over the discrete Fourier transform. In fact, for some data sets with data gaps or missing data, it is the only method to calculate spectral information short of making up bogus data to fill the gaps. The prime disadvantage of the periodogram is that it takers longer to compute than an FFT.

First, the mean of the original time series of variable A is subtracted from each A(k) data point to yield a modified time series for A'(k). For each frequency (n) a wave of the following form is fitted to the data:

$$A' = a_1 \cos\left[\frac{2\pi kn}{N}\right] + a_2 \sin\left[\frac{2\pi kn}{N}\right] \qquad (8.9a)$$

where A' is the deviation of A from the mean, and where a_1 and a_2 are the best-fit coefficients to be determined. Solving for a_1 and a_2 (both a function of n) in the least-squares sense gives:

$$a_1 = \frac{\overline{A's'}\,\overline{s'c'} - \overline{A'c'}\,\overline{s'^2}}{(\overline{s'c'})^2 - \overline{c'^2}\,\overline{s'^2}} \quad \text{and} \quad a_2 = \frac{\overline{A'c'}\,\overline{s'c'} - \overline{A's'}\,\overline{c'^2}}{(\overline{s'c'})^2 - \overline{c'^2}\,\overline{s'^2}} \tag{8.9b}$$

where

$$s' = \sin[2\pi nk/N] - \overline{\sin[2\pi nk/N]} \quad \text{and} \quad c' = \cos[2\pi nk/N] - \overline{\cos[2\pi nk/N]}$$

and where the overbar denotes an average over all N data points of the original time series. In the definitions of s' and c' above, note that the overbar terms in each expression are identically equal to zero only for n equal to an integer value.

Given the best fit from above, we can compute the correlation coefficient squared, $r^2(n)$:

$$r^2(n) = \frac{\text{explained variance}}{\text{total variance}} = \frac{a_1\,\overline{A'c'} + a_2\,\overline{A's'}}{\overline{A'^2}} \tag{8.9c}$$

If waves at frequency n explain a lot of variance in the original signal, then $r^2(n)$ is close to 1. Otherwise, it is closer to zero. For integer values of n, $r^2(n)$ is equal to the normalized spectral intensity, $E_A(n)/s_A^2$, of the FFT. This is where the spectral information comes from.

We must solve (8.9b & c) many times, for each different value of n that we are interested in. To calculate a complete spectra, we should solve the equation for at least the N different integer values of n. Thus, when $r^2(n)$ is plotted vs. n, the result is a spectrum. As an example, the spectra plotted in section 8.7 could have been labeled as r^2 vs n, where r^2 would have been computed using periodogram methods. Note that we can also solve the equations for noninteger values of n, and for n in the range 0 to 1, if desired, although sine waves of noninteger values are not mutually orthogonal.

8.10 Nonlocal Spectra

Contained within the nonlocal-closure transilient matrix is information about the amount of fluid that mixes between each pair of grid-point locations in a column of air during a finite time. This information can be extracted and grouped to yield spectral information about the contributions of different wavelengths to the overall mixing ***process.*** Such a spectrum differs from the spectrum of the fluid ***state*** obtained from harmonic analysis (FFT) of measurements of temperature, velocity or other state variables, as described in all the previous sections of this chapter. Tennekes (1976) pointed out that the FFT Fourier modes do not have a one-to-one correspondence with eddies.

8.10.1 Transport Spectra

The turbulent flux is the result of a turbulent process. Without the process of eddies moving and mixing various air parcels, there would be no turbulent flux regardless of the state of the air. Transport spectra are based on fluxes, while state spectra (FFTs) are based on variances.

To see how transport spectra (TS) are related to the transilient turbulence theory, start with the definition for kinematic flux given by (6.8.4b). Instead of summing over the contributions from ALL pairs of grid points within the domain of turbulence, as specified in (6.8.4a), we can selectively sum over only those pairs of points having a specified separation distance (i.e., wavelength). If we let $m \cdot \Delta z$ equal the wavelength of interest, then the portion of flux associated with wavelength-index m that contributes to the total flux at height-index k (i.e., at height $z = k \cdot \Delta z$) is:

$$TS(k,m) = \frac{\Delta z}{\Delta t} \sum_{i=1}^{k} \sum_{j=k+1}^{N} \delta_{m,|i-j|} \left[c_{ji} \bar{\xi}_i - c_{ij} \bar{\xi}_j \right] \qquad (8.10.1a)$$

where δ_{ij} is the usual Kronecker delta, Δz is the vertical grid increment, Δt is the timestep increment, and m is an integer between 1 and N.

The total flux at location k is given by the sum of transport spectra over all wavelengths:

$$\overline{w'\xi'}(k) = \sum_{m=1}^{N} TS(k,m) \qquad (8.10.1b)$$

It is always a good check to use (8.10.1b) confirm that the sum of the transport-spectral components does indeed equal the total flux.

A case-study example of a transport spectrum is shown in Fig 8.13 for the kinematic heat flux at two different heights within the turbulent boundary layer near the Cabauw tower in the Netherlands at 1500 UTC, 30 May 1978 (Stull and Driedonks, 1987). A 3 km column of air near the tower is modeled using 30 grid boxes, each 100 m thick. The mixed layer within this column at 1500 UTC was about 2100 m thick.

At a height of z = 100 m (i.e., at k = 1) we find that the smallest resolved wavelengths contribute most the the heat flux for this case, while the wavelengths of the range 1000 m to 2000 m make a smaller, but yet significant, contribution. At a height of 500 m above ground the smallest wavelengths contribute virtually nothing to the total flux, while wavelengths in the 500 m to 1700 m range dominate. At both of these heights, it is interesting to see that the largest wavelength within the turbulent domain has a negative contribution to the total heat flux. This is associated with the entrainment of warm air downward by the thermal-scale eddies.

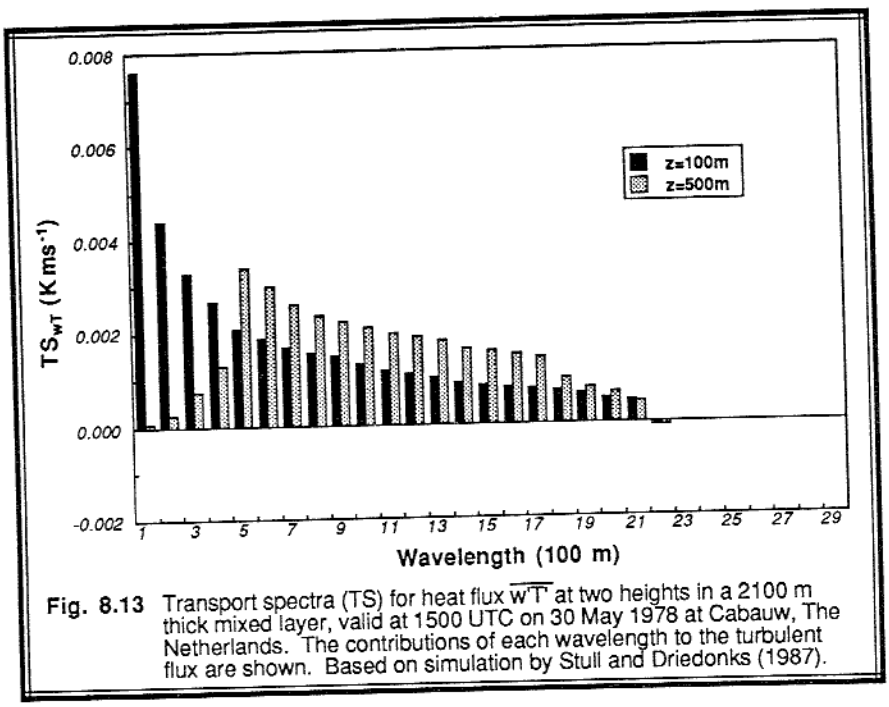

Fig. 8.13 Transport spectra (TS) for heat flux $\overline{w'T'}$ at two heights in a 2100 m thick mixed layer, valid at 1500 UTC on 30 May 1978 at Cabauw, The Netherlands. The contributions of each wavelength to the turbulent flux are shown. Based on simulation by Stull and Driedonks (1987).

8.10.2 Process Spectra

One limitation of transport spectra is that the flux contribution can be small even if the mixing process is vigorous. This can happen when the difference of the variable values between the heights being mixed is small or zero. To help focus on the mixing process alone, we can define a ***process spectrum*** that does not use the values of the variable being mixed:

$$PS(k,m) = \sum_{i=1}^{k} \sum_{j=1}^{N} \delta_{m,|i-j|} \, c_{ij}(t,\Delta t) \qquad (8.10.2a)$$

One expects this spectrum to be the same for heat, moisture, tracers, and maybe for momentum (neglecting pressure effects and waves), because it describes the mixing process rather than the effect of the mixing on the fluid state.

Fig 8.14 shows a process spectrum for the same Cabauw case as Fig 8.13. As before, the smallest wavelengths are the most important at the lowest height. As height increases, the peak in the spectrum becomes broader, less peaked, and shifts to longer wavelengths.

This behavior is related to mechanisms that generate turbulence. Near the surface, strong superadiabatic lapse rates and wind shears create strong dynamic instabilities across

short distances, to which the transilient parameterization described in Chapter 6 responds with vigorous mixing at small wavelengths. Near the entrainment zone, however, the lapse rate is locally stable, suppressing generation of small-scale mixing except by wind shear. The largest scales continue to be slightly unstable near the entrainment zone, associated with warm thermals rising from the surface layer.

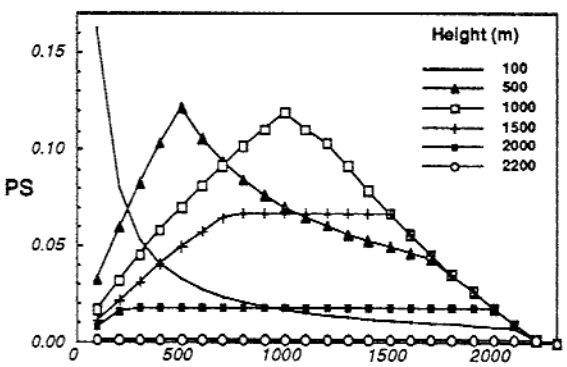

Fig. 8.14 Process spectra (PS) for the same case as Fig. 8.13, showing the contribution of each wavelength to the total mixing at the indicated height.

Prandtl (1925) recognized that eddies of a variety of sizes can simultaneously operate at any point in the turbulent domain. Due to lack of computer power in the early 1900s, he suggested averaging over the spectrum of eddy sizes to yield one mixing length for each point in space. At the time he had no real measure of the relative importance to the overall mixing length of the various eddy sizes. Instead, he parameterized the mixing length directly as a function of boundary layer and turbulence scales, as discussed in Chapter 6.

We can use the process spectrum to examine the relative importance of various scales of mixing to the overall mixing length by applying the process-spectral amplitudes as weights for their respective wavelengths. The resulting weighted wavelength is like a mixing length, l, which we can find at each height ($z = k \cdot \Delta z$):

$$l(k) = \Delta z \cdot \frac{\sum_{m=1}^{N} m \cdot PS(k,m)}{\sum_{m=1}^{N} PS(k,m)} \qquad (8.10.2b)$$

Fig 8.15 shows mixing lengths as a function of height for the same Cabauw case study. The mixing length increases with height in the bottom of the mixed layer, but

becomes nearly constant with height in the top half of the mixed layer. The mixing length is undefined in the nonturbulent air above the mixed layer, because the process spectral amplitudes are zero.

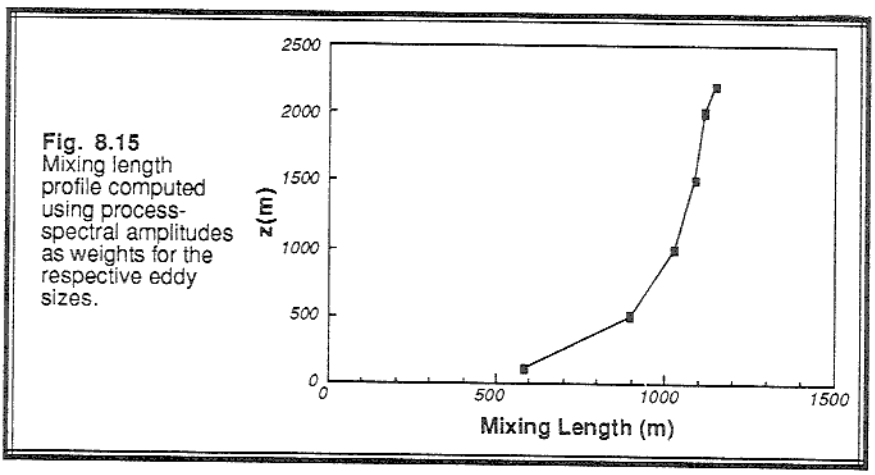

Fig. 8.15 Mixing length profile computed using process-spectral amplitudes as weights for the respective eddy sizes.

8.11 Spectral Decomposition of the TKE Equation

8.11.1 Spectral Decomposition Methods

Although we have concentrated on discrete spectral methods in this chapter, an obvious extension is to use integrals to describe the Fourier transform pair for continuous functions. In the following example, we will decompose the original function A(t,x) into a Fourier integral in a single spatial direction, x, but will not perform a similar decomposition in time. For this case, the Fourier transform pair is:

Inverse Transform

$$A(t,x) = \int_{\kappa=-\infty}^{\infty} F(t,\kappa)\, e^{i\kappa x}\, d\kappa \qquad (8.11.1a)$$

Forward Transform

$$F(t,\kappa) = \frac{1}{2\pi} \int_{x=-\infty}^{\infty} A(t,x)\, e^{-i\kappa x}\, dx \qquad (8.11.1b)$$

where κ is wavenumber.

Substitution of (8.11.1a) into a term like $\partial A(t,x)/\partial x$ yields:

$$\frac{\partial A(t,x)}{\partial x} = \frac{\partial}{\partial x} \int_{\kappa} F(t,\kappa)\, e^{i\kappa x}\, d\kappa = \int_{\kappa} F(t,\kappa) \frac{\partial\, e^{i\kappa x}}{\partial x}\, d\kappa = \int_{\kappa} F(t,\kappa)\, i\, \kappa\, e^{i\kappa x}\, d\kappa$$

On the other hand, a term like $\partial A(t,x)/\partial t$ becomes:

$$\frac{\partial A(t,x)}{\partial t} = \int_{\kappa} \frac{\partial F(t,\kappa)}{\partial t} e^{i\kappa x} d\kappa$$

As an example of how this is used in complete equations, start with the simple advection equation with constant mean wind,

$$\frac{\partial A(t,x)}{\partial t} = -\overline{U} \frac{\partial A(t,x)}{\partial x}$$

and spectrally decompose it to yield:

$$\int_{\kappa} \frac{\partial F(t,\kappa)}{\partial t} e^{i\kappa x} d\kappa = -\overline{U} \int_{\kappa} F(t,\kappa)\ i\kappa e^{i\kappa x} d\kappa$$

An integral over wavenumbers appears in every term of the above equation. Thus, we could focus on the contribution of any ONE wavenumber to the whole equation by looking at the respective integrands (moving $\overline{U}$ under the integral because it is not a function of κ):

$$\frac{\partial F(t,\kappa)}{\partial t} e^{i\kappa x} = -\overline{U} \quad F(t,\kappa)\ i\kappa e^{i\kappa x}$$

The factor $\exp(i\kappa x)$ appears in every term of the above equation, and can be cancelled out. This leaves use with a spectral representation of the advection equation:

$$\partial F(t,\kappa) / \partial t = -\overline{U}\ i\kappa F(t,\kappa)$$

As you have probably anticipated, we could let A(t,x) represent a variable like perturbation velocity, u'(t,x), or perturbation potential temperature, $\theta'(t,x)$. Thus we can use the same general approach as show above to spectrally decompose the TKE equation.

8.11.2 Spectral Representation of the TKE Equation

Since the spectral decomposition of the TKE equation is somewhat complex, the reader is referred to Batchelor (1953) and Borkowski (1969) for the details. The end result for homogeneous turbulence, where S is the spectral energy, is:

$$\frac{\partial S(t,\kappa)}{\partial t} = \frac{g}{\theta_v}\,\gamma(t,\kappa) - \phi(t,\kappa)\frac{\partial \overline{U}}{\partial z} + \frac{\partial Tr(t,\kappa)}{\partial \kappa} - 2\nu\,\kappa^2\,S(t,\kappa) \qquad (8.11.2)$$

I III IV V(κ) VII

Term I The local time tendency of the κ^{th} spectral component of the TKE

Term III Buoyant production or loss associated with the κ^{th} component of $\overline{w'\theta_v'}$

Term IV Mechanical (shear) production associated with the κ^{th} component of $\overline{u'w'}$

Term V(κ) Convergence of TKE transport across the spectrum

Term VII Viscous dissipation of the κ^{th} component of TKE

This equation was the one referenced in section 5.3, where the relative contributions of the four terms on the right of (8.11.2) were plotted. When integrated over wavenumbers from 0 to ∞, the result is the TKE equation (5.1b).

The individual factors are defined as follows: $TKE = \int S(t,\kappa)\,d\kappa$, $\overline{w'\theta_v'} = \int \gamma(t,\kappa)\,d\kappa$, $\overline{u'w'} = \int \phi(t,\kappa)\,d\kappa$, and $\varepsilon = 2\nu \int \kappa^2\, S(t,\kappa)\,d\kappa$, where the integrals are from 0 to ∞. The transport term $\partial Tr/\partial\kappa$ becomes zero when integrated across the spectrum, because it represents the transport of existing TKE from the low wavenumber portions of the spectrum (where energy is produced) to the high wavenumber regions (where it is dissipated).

In the inertial subrange portion of the spectrum where there is neither production nor dissipation, we would expect that the transport across the spectrum, $Tr(t,\kappa)$ would be equal in magnitude to the total dissipation rate: $Tr(t,\kappa) = \varepsilon$. This transport is nothing more than the ***energy cascade*** that was introduced early in the text.

8.12 References

Batchelor, G.K., 1953: *The Theory of Homogeneous Turbulence*. Cambridge Univ. Press, London.

Bergland, G.D., 1969: A guided tour of the fast Fourier transform. *IEEE Spectrum*, **6**, 41-51.

Borkowski, J., 1969: Spectra of anisotropic turbulence in the atmosphere. Proceedings of Colloquium on Spectra of Meteorological Variables, Stockholm, June 9-19, 1969. *Radio Science* (Dec 1969), **4**, 1351-1355.

Deardorff, J.W. and G.E. Willis, 1985: Further results from a laboratory model of the

convective planetary boundary layer. *Bound.-Layer Meteor.*, **32**, 205-236.

Jenkins, G.M., and D.G. Watts, 1968: *Spectral Analysis and Its Applications*, Holden-Day, Oakland, CA. 523pp.

Lenschow, D.H., 1986: *Probing the Atmospheric Boundary Layer*. American Meteorological Society, Boston, MA. 269pp.

Lumley, J.L. and H.A. Panofsky, 1964: *The Structure of Atmospheric Turbulence*. Interscience Publishers (Wiley), New York. 239pp.

Neff, W.D. and R.L. Coulter, 1986: Acoustic remote sensing. *Probing the Atmospheric Boundary Layer*, D.H. Lenschow (Ed.), American Meteor. Society, Boston. 201-239.

Otnes, R.K. and L. Enochson, 1972: *Digital Time Series Analysis*. Wiley-Interscience, New York. 467pp.

Panofsky, H.A., and G.W. Brier, 1968: *Some Applications of Statistics to Meteorology*, Penn State Univ., University Park, PA. 224pp.

Panofsky, H.A. and J.A. Dutton, 1984: *Atmospheric Turbulence, Models and Methods for Engineering Applications*. John Wiley (Wiley-Interscience Pub.), New York. 397pp.

Prandtl, L., 1925: Bericht über Untersuchungen sur ausgebildeten Turbulenz. *Zs. angew. Math. Mech.*, **5**, 136-139.

Priestley, M.B., 1981: *Spectral Analysis and Time Series, Vols 1 & 2*. Academic Press, New York. 490 pp.

Stull, R.B. and A.G.M. Driedonks, 1987: Applications of the transilient turbulence parameterization to atmospheric boundary-layer simulations. *Bound.-Layer Meteor.*, **40**, 209-239.

Tennekes, H., 1976: Fourier transform ambiguity in turbulence dynamics. *J. Atmos. Sci.*, **33**, 1660-1663.

Wyngaard, J.C., Y. Izumi, and S.A. Collins, Jr., 1971: Behavior of the refractive index structure parameter near the ground. *J. Opt. Soc. Am.*, **61**, 1646-1650.

Wyngaard, J.C. and M.A. LeMone, 1980: Behavior of the refractive index structure parameter in the entraining convective boundary layer. *J. Atmos. Sci.*, **37**, 1573-1585.

8.13 Exercises

1) Given the following set of turbulence velocity measurements, find the autocorrelation function using both the exact and approximate formulae. These measurements were taken every second:
   5.5, 6.3, 7.4, 3.3, 3.8, 5.9, 6.1, 5.7, 6.3, 7.1, 4.8, 3.1, 2.1, 2.4, 3.0
   Plot this time series and your autocorrelation functions on separate graphs. What is the difference between the exact and approximate autocorrelation curves?
2) Compute the structure function vs lag, for the data of problem 1. Plot and discuss your results. Find the structure function parameter. Discuss the quality of the fit of (8.3.1b) to this data set.
3) Theoretically prove that if $A(t) = \sin(t)$, then $R(L) = \cos(L)$.
4) Prove analytically the following relationship between structure function and autocorrelation: $D(L) = \sigma_x^2 [1-R(L)]$. Assume stationary turbulence (i.e., σ_x^2 is constant).
5) Compute the exact autocorrelation and structure function for the following data set, and plot your results for lags from 0 through 180 s. Discuss how the shape of the original time series compares with the peaks in the autocorrelation curve.

t(s)	T(C)	w(m/s)	t(s)	T(C)	w(m/s)
0	25	2			
10	23	2	110	20	-4
20	21	-1	120	19	-1
30	21	1	130	20	1
40	30	4	140	25	3
50	20	-3	150	21	0
60	24	3	160	25	1
70	23	1	170	23	0
80	23	2	180	21	-2
90	24	3	190	20	-1
100	23	-1	200	19	-2

6) Compute the discrete Fourier transform for the time series from problem 1. Instead of using a canned FFT package, write your own program or develop a spreadsheet to solve it. Check your results by doing an inverse FFT to reconstruct the data set. Also check to see that the sum of the spectral energies equals the biased variance of the original signal. Compute and plot the spectrum.
7) Compute the discrete Fourier transform for the time series from problem 1, using a canned FFT program. If you solved problem 6, how do your answers compare.
8) Prove mathematically that sine waves of different integer frequencies, n, are orthogonal to each other. By orthogonal, we mean that a wave with one n value cannot be described by a sum of waves with other n values. As an alternative, test the orthogonality with some specific cases. For example, define A(k) as a sine wave with n=2. Then see if the discrete Fourier transform of this wave has any energy at n=3.

9) Compute the individual FFTs for the two data sets from problem 5, using canned statistical packages. Compare the simple spectrum for T with that for w.
10) Using the FFT temperature output from problem 9, set the 5 frequencies nearest the Nyquist frequency to zero, on both sides of the Nyquist frequency. Do this to the Fourier transform itself, not to the spectrum. Then use this modified phase space data to compute an inverse transform. Plot the resulting physical space time series, along with the original temperature time series from problem 5. What you have just done was an ideal low-pass filter.
11) Use the FFT output from problem 9 to manually compute (or use a spreadsheet) the cross spectral information: cospectrum, quadrature spectrum, coherence, amplitude, and phase spectra. If you have a canned statistical package that also computes these values, compare the results.
12) Compute a new time series of w'T' values from the data in problem 5. Calculate the covariance for this series, and then do an FFT on the series. Compare the resulting simple spectrum from this FFT output with the cross spectral results from problem 11.
13) Write a program to compute the periodogram. Use it to find the spectrum (r^2 values vs. n) for the data in problem 1, for n values ranging from 0.1 to 10, with increments of $\Delta n = 0.2$. Compare the r^2 values for integer n with the spectral output from problem 6 normalized by the total variance.
14) If you have an odd number of data points in a time series vs. an even number, how does that affect the Nyquist frequency?
15) When the spectral form of the TKE equation (8.6.2) is integrated over wavenumber from 0 to ∞, the result is close to the TKE equation (5.1b).
(a) Discuss the differences.
(b) Also, if (8.6.2) is integrated over wavenumbers from 0 to κ_{IS}, where κ_{IS} is in the middle of the inertial subrange, then describe the physical relationships and magnitudes of the resulting integrated terms.
16) Write a computer program to generate a time series consisting of 10 oscillations of a perfect sine wave within a 1-minute period. Sample this series 18 evenly-spaced times during that same period. Plot this sampled time series, and discuss the shape in relation to the Nyquist frequency and aliasing.
17) Prove mathematically that the Fourier transform results are also the best-fit sine and cosine waves in the least-squares sense.
18) Use the Profile B data and the transilient matrix from example 6.8.5 to calculate the the transport and process spectra for all wavelengths (m = 1 to 5) for heights z = 100, 200, and 300 m, and plot your results on separate graphs.
19) Spectrally decompose equation (3.5.3c). Comment on the wavenumber dependence of advection terms (both turbulent and mean).